225166

UCRL-JC-118254
PREPRINT

A Simple Model of Photon Transport

Dermott E. Cullen
Department of Physics
University of California
Lawrence Livermore National Laboratory
Livermore, CA 94550

This paper was prepared for submittal to
Nuclear Instruments and Methods
in Physics Research
Section B

July 1994

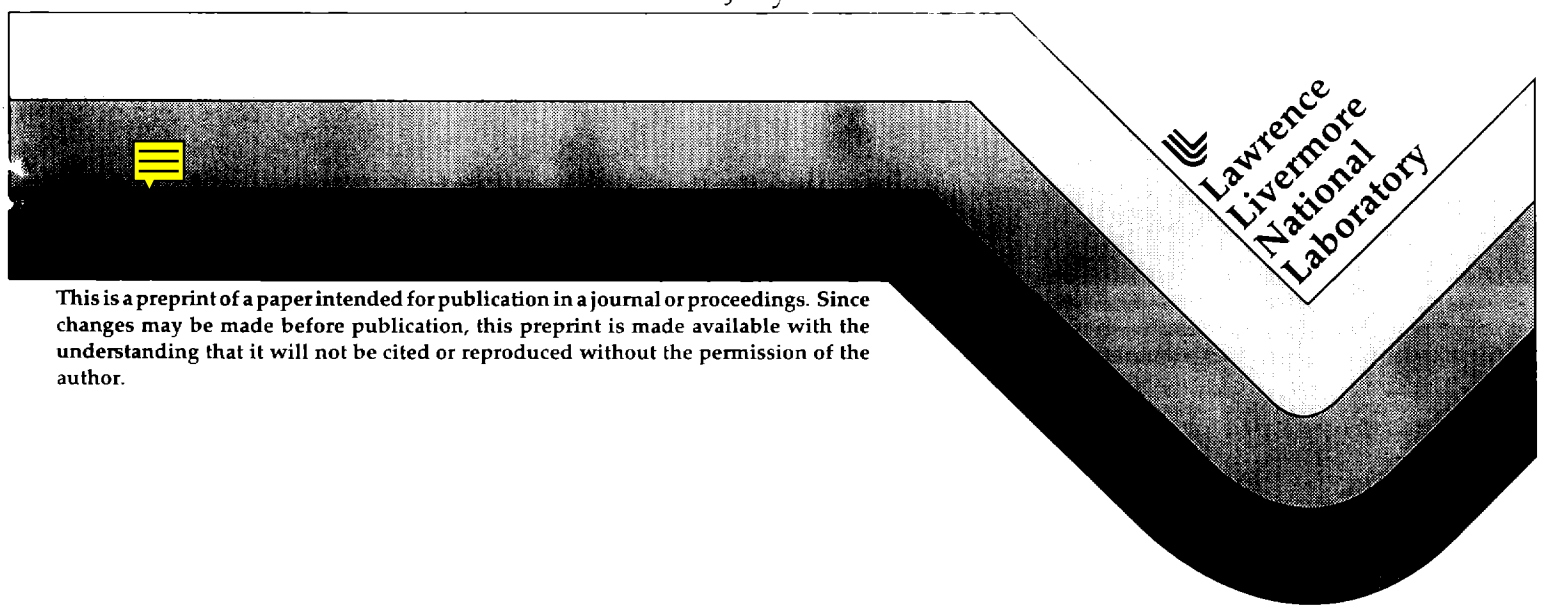

A Simple Model of Photon Transport

by

Dermott E. Cullen
Lawrence Livermore National Laboratory
L-294, P.O. Box 808
Livermore, Ca 94550

July 1994

Overview

In this paper I describe a simple model of photon transport. This simple model includes: tabulated cross sections and average expected energy losses for all elements between hydrogen (Z = 1) and fermium (Z = 100) over the energy range 10 eV to 1 GeV, simple models to analytically describe coherent and incoherent scattering, and a simple model to describe fluorescence. This is all of the data that is required to perform photon transport calculations.

Each of these simple models is first described in detail. Then example results are presented to illustrate the accuracy and importance of each model.

These models have now been implemented in the Epic (Electron Photon Interaction Code). All of the figures and results presented here are from Epicshow, an interactive program to allow access to the Epic data bases, and Epicp, a simple photon transport code designed to develop optimum algorithms for later use in Epic. Epicp is made up of four parts: 1) a simple unoptimized driver to perform transport calculations, 2) an i/o package to handling reading of the binary, random access data files, 3) a physics package to handle kinetics of all processes, 4) a utility package containing all computer dependent routines, e.g., define running time, initialize random number sequence, etc. The focus is on optimizing parts 2) and 3) for later use in Epic; these are the parts that are of general interest, since they can be used in any photon transport code. Epicshow and Epicp and the Epic data bases are now available from the author.

Treatment of Integral Parameters

In this section, I discuss the treatment of integral parameters, which includes: total photoelectric, coherent and incoherent scattering, pair and triplet production cross sections, photoelectric subshell cross sections, and expected energy deposition for photoelectric, incoherent scattering, pair and triplet production.

The data used is based on the Livermore Evaluated Photon Data Library (EPDL), which includes data for all elements between hydrogen (Z = 1) and fermium (Z = 100), over the energy range 10 eV to 100 GeV[1]. This data has been adopted as the ENDF/B-VI Photon Interaction Library [2], but at the request of the Cross Section Evaluation Working Group (CSEWG), the ENDF/B-VI data has been restricted to the energy range 10 eV to 100 MeV.

In addition to the basic integral cross sections describing coherent, incoherent, photoelectric, pair and triplet production, EPDL also includes photoelectric cross sections for each atomic subshell and expected energy deposits for each process. EPDL also includes form factors and scattering functions to describe coherent and incoherent scattering, respectively. The ENDF/B-VI library includes the photoelectric subshell cross sections, form factors and scattering functions, but not expected energy deposits (there are no ENDF/B formats for these quantities).

In evaluating the EPDL data, each physical process for each element was considered separately. The result is data represented on a different energy grid for each process and each element and generally requiring log-log interpolation between the tabulated results. Using this data in this form in applications would be extremely cumbersome, very expensive and simply not practical.

For use in applications the data has been reduced to simple tabulated form. For each element, all cross sections and average expected energy deposits are all in a simple tabulated form where all parameters are tabulated at the same energies and the tabulated energy points have been selected to allow linear interpolation to any energy between any two tabulated points. At the request of users, the energy range has been extended from the ENDF/B-VI upper limit of 100 MeV, up to 1 GeV.

Table 1 illustrates the Epic photon cross sections for lead in exactly the simple tabulated form that they are distributed. The first line defines Z, the number of tabulated points, the atomic weight and STP density of the element, and the chemical symbol. The second line identifies each column that follows: energy in MeV, six cross sections in barns, expected energy deposit per collision in MeV(note, the photoelectric energy deposit is the incident energy minus fluorescence energy = what is considered to be deposited locally). There are 100 such tables, one after the other for Z = 1 through 100. There is a similar file of data for the subshell cross sections, form factor and scattering function parameters, and fluorescence yields. For use in applications, all of these files are combined into a single binary, random access file.

The systematic variation of the photoelectric edges as a function of atomic number (Z) does not allow the data for all of the elements to be accurately represented on a common energy grid for all elements. This point will be discussed below.

Once the data for each element has been reduced to the simple tabulated form, described above, where all parameters are represented on exactly the same energy grid, and can be accurately represented using linear interpolation between tabulated points, a very efficient and almost trivial binary search can be used to define the tabulated energy interval within which the current energy lies. Once this is done, ALL of the parameters for the elements can be defined as a simple weighted sum of the contributions from the two tabulated values at the end of the interval. For example, assume that the current energy, E, lies between the tabulated energies, E_{j-1} and E_j. If we define the weights,

$$\begin{aligned} Weight_j &= \left[E - E_{j-1}\right] / \left[E_j - E_{j-1}\right] \\ Weight_{j-1} &= 1 - Weight_j \end{aligned} \qquad (1)$$

then ANY and ALL parameters can be defined at energy, E, as,

$$F(E) = Weight_j * F_j + Weight_{j-1} * F_{j-1} \quad (2)$$

where F is any parameter of interest, e.g., photoelectric or pair production cross section, incoherent or photoelectric energy deposit, K or L1 photoelectric subshell cross section, etc.and F_{j-1}, and F_j are the tabulated values of F at E_{j-1} and E_j, respectively.

To represent all of the data over the entire energy range from 10 eV up to 1 GeV and allow accurate linear interpolation between tabulated points requires no more than 255 points for any given element. In creating the files, no attempt was made to keep the number of points under this limit; it just happened naturally. But the result is obviously ideal for facilitating a quick and efficient binary search.

Formerly, people have attempted to fit the photon interaction cross sections to analytical expressions that could be used in applications. This approach worked quite well to represent the basic cross sections and has been very successfully used in the past.

If we wish to perform more detailed photon transport calculations where we require more detailed information, such as photoelectric subshell cross sections, over more extended energy ranges, the approach of using analytical expressions becomes impractical

In the case of the approach used here, a combination of 19 different cross sections and energy depositions can ALL be defined at any given energy as this simple weighted average of two tabulated terms. If one attempted to fit all of this data to analytical expressions and then had to evaluate each of the analytical expressions at each energy during a transport calculation, it seems clear which approach would be both faster and more accurate, i.e., the old approach of using analytical expressions simply is not practical to use for more detailed calculations.

Photon Scattering

In the following sections, discussing photon scattering, we will only be interested in developing methods to efficiently sample the normalized scattering distributions. We assume that the cross section for each process has already been defined and what we are interested in is: given that a coherent or incoherent scattering event has occurred (based on the cross sections), what is the angular, and in the case of incoherent also the energy, distribution of the scattered photons.

Below, we will see that based on the equations describing coherent and incoherent scattering, the most "natural" angular variable to use is neither angle nor σ, but rather $1 - \sigma$; and more generally $E^2 (1 - \sigma)$.

Coherent Scattering

The angular distribution of coherently scattered photons is a product of Rayleigh scattering and a correction factor,

sig(cos) = R(cos)*f(E,cos)

R(cos) = Rayleigh scattering

f(E,cos) = correction factor

E = incident photon energy

cos = photon scattering σ

$R(\cos) = [\cos^2 + 1]$

$= [2 - x * (2 - x)], x = 1 - \cos$

$$f(E,\cos) = [FF(E,\cos) + AS(E)]^2 \qquad (4)$$

FF(E,cos) = the Form Factor

AS(E) = the Anomalous Scattering Factor

The anomalous scattering factor plays an important role by creating minima in the coherent scattering cross section just below photoelectric edges and in causing the coherent scattering cross section to approach zero as E^2 as energy approaches zero [3].

It plays a less important role in that it effects the angular distribution of coherently scattered photon near photoelectric edges.

The important effect of the anomalous scattering factor on the coherent cross section has been included in the EPDL cross sections. The less important effect of the anomalous scattering factor on the angular distributions near photoelectric edges will be ignored here; so that we assume,

$$f(E,\cos) = FF(E,\cos^2) = \textit{Form Factor squared} \qquad (5)$$

Generally for use in applications, the form factor is represented in tabulated form that is then fit by some procedure (e.g., cubic spline) and sampled.

Here we will use an analytical expression that is simpler and more efficient to sample.

For a hydrogen atom the form factor is (4),

$$FF(E,\cos) = Z / [1 + B * x]^2, x = \mathrm{E}^2 * (1 - \cos) \tag{6}$$

For more complicated atoms, the form form factor can be presented by a sum of terms, with each term corresponding to the contribution of each atom subshell j,

$$FF(E,\cos) = \sum_j Aj / [1 + Bj * x]^{Nj} \tag{7}$$

so that the form factor squared, that we need for use in applications, can be represented in the form,

$$FF(E,\cos^2) = \sum_j Aj / [1 + Bj * x]^{Nj} * \sum_k Ak / [1 + Bk * x]^{Nk} \tag{8}$$

This form is judged to be too complicated and expensive to use in Monte Carlo calculations. So we will use the pragmatic approach of representing the form factor in the form,

$$FF(E,\cos)^2 = \sum_j Aj / [1 + Bj * x]^N \tag{9}$$

and use Aj, Bj and N as free parameters to fit tabulated form factors. N is easily defined by examining the high energy shape of the form factor, where,

Bj*x >> 1

in which case the shape is given by,

$$\sum_j Aj / [Bj * x]^N = C / [x]^N, where\ C = \sum_j Aj / Bj^N \tag{10}$$

so that N is merely the high energy log slope of the form factor. Aj and Bj are then defined to obtain the best fit to the form factor.

In the normally used definition of the form factor, it varies from Z at low energy to 0 at high energy. Since here we are fitting the square of the form factor, the one constraint that we have is,

$$Z^2 = \sum_j Aj \tag{11}$$

It has been found that the tabulated EPDL form factors can be very accurately fit using no more than a sum of three terms. For hydrogen and helium where we only have one atom shell (K), only one term is required. For Z = 3 To 10, we have K and L shells, and only two termsare required.

For higher Z elements more terms are required as the effect of each subshell can be seen. However, since generally coherent scattering is described as an interaction between a photon and the inner most, most tightly bound electrons of an atom we do not see a sum corresponding to contributions from each subshell; the sum seems to saturate and involve contributions from only up to three discernible terms. The power N varies smoothly from 4 for hydrogen(Z = 1) to about 2.43 for ferium (Z = 100).

Figs. 1 and 2 illustrate comparisons between the original EPDL form factors and the fits that can be used in applications. These figures illustrate results for elements across the periodictable, Z = 1, 10, 20, 30, 40, 60, 80 and 100. The results indicate that these simple fits can be used to approximate the square of the form factor over ten to twelve decades of variation, i.e., well beyond the range that we can normally statistically sample.

As can be seen from these figures, at low energy the form factor is virtually isotropic and sampling only involves sampling the Rayleigh cross section. However, at higher energies the form factors are very strongly forward peaked and dominate the definition of the angular distribution of coherently scattered photons.

This suggests using a rejection technique to first analytically sample the form factor and then accept or reject based on the Rayleigh cross section.

The integral of each term of our fit is,

$$P' = \int_0^y Aj * dy' / [1 + Bj * E^2 * y']^N = \left[Aj / (Bj * E^2)\right] * \left\{1 - 1 / [1 + Bj * E^2 * y]^{N-1}\right\} / (N - 1) \tag{12}$$

$$\frac{Aj * \left[(1 + Bj * E^2 * y)^{N-1} - 1\right]}{(N-1) * Bj * E^2 * \left[(1 + Bj * E^2 * y)^{N-1}\right]} = \tag{13}$$

The normalization is defined by setting y = 1 - cos = 2,

$$\frac{Aj * \left[(1 + Bj * E^2 * 2)^{N-1} - 1\right]}{(N-1) * Bj * E^2 * \left[(1 + Bj * E^2 * 2)^{N-1}\right]} = \tag{14}$$

The normalization can be calculated in advance for each of the terms of the fit as a function of incident energy at the same energies at which the cross sections are tabulated. Then when a coherent scatter occurs, these tabulated normalizations can be used to quickly randomly select one of the three terms based on its normalization, i.e., its contribution to the sum of terms.

From this point on, we need only be concerned with randomly sampling the one term of the series that we have selected. The normalizedform for one term is.

$$\frac{\left[Aj/\left(Bj*E^2\right)\right]*\left\{1-1/\left[1+Bj*E^2*y\right]^{N-1}\right\}/(N-1)=}{\left[Aj/\left(Bj*E^2\right)\right]*\left\{1-1/\left[1+Bj*E^2*2\right]^{N-1}\right\}/(N-1)} \tag{15}$$

$$\frac{\left\{1-1/\left[1+Bj*E^2*y\right]^{N-1}\right\}=}{\left\{1-1/\left[1+Bj*E^2*2\right]^{N-1}\right\}} \tag{16}$$

The scattering angle is then defined by analytically inverting and solving for y (y = 1 - cos),

$$\left\{1-1/\left[1+Bj*E^2*y\right]^{N-1}\right\}$$

$$P=\frac{}{\left\{1-1/\left[1+Bj*E^2*2\right]^{N-1}\right\}},\ P\ =\ a\ random\ number,\ 0\ to\ 1 \tag{17}$$

$$\begin{aligned} &Define,\ Q=Bj*E^2\\ &\qquad D=1+2*Q\\ &\qquad E=1+y*Q\\ &\qquad C=1/\left[1-1/D^{N-1}\right] \end{aligned} \tag{18}$$

$$P\qquad\qquad=\left\{1-1/E^{N-1}\right\}/\left\{1-1/D^{N-1}\right\}$$

$$\left\{\left[1-1/D^{N-1}\right]*P=1-1/E^{N-1}\right\}$$

Inverting and solving for y,

$$y=\frac{\left\{D-\left[P+(1-P)*D^{N-1}\right]\left[1/(N-1)\right]\right\}}{Q*\left[P+(1-P)^{N-1}\right]\left[1/(N-1)\right]} \tag{19}$$

The above equations may seem complicated, but the entire sampling only involves, select a random number P, and then define,

$$
\begin{aligned}
&Q = Bj * E^2 \\
&D = 1 + 2 * Q \\
&F = \left[P + (1-P) * D^{N-1}\right] \left[1/(N-1)\right] \\
&y = [D - F] / [Q * F]
\end{aligned}
\tag{20}
$$

The two limits of P = 0 and P = 1 can be easily seen to correspond to,

$$
\begin{aligned}
&P = 0 \\
&F = D \\
&y = [D - D] / [Q * D] \quad = 0 \quad = 1 \; - \; \cos,\ \cos = +1
\end{aligned}
\tag{21}
$$

$$
\begin{aligned}
&P = 1 \\
&F = 1 \\
&y = [D - 1] / Q = 2 * Q / Q = 2 = 1 - \cos,\ \cos \; = \; -
\end{aligned}
\tag{22}
$$

At low energy, where,

$$
\begin{aligned}
&Q = Bj * E^2 << 1 \\
&D = 1 + 2 * Q
\end{aligned}
$$

We can expand terms,

$$D^{N-1} \qquad \sim 1 + 2 * (N - 1) * Q \tag{24}$$

$$
\begin{aligned}
P + (1-P) * D^{N-1} \qquad &\sim P + (1-P) * [1 + 2 * (N-1) * Q] \\
&\sim 1 + (1-P) * 2 * (N-1) * Q
\end{aligned}
\tag{25}
$$

$$\left[P + (1-P) * D^{N-1}\right] \left[1/(\mathrm{N}-1)\right] \qquad \sim 1 + (1-P) * 2 * Q \tag{26}$$

$$D - \left[P + (1-P) * D^{N-1}\right] \left[1/N - 1\right] \sim 1 + 2 * Q - \left[1 + (1-P) * 2 * Q\right]$$
$$\sim 2 * Q * \left[1 - (1-P)\right] \qquad (27)$$
$$\sim 2 * Q * P$$

$$y \sim 2 * Q * P / \left\{Q * \left[1 + (1-P) * 2 * Q\right]\right\}$$
$$\sim 2 * P / \left[1 + (1-P) * 2 * Q\right] \qquad (28)$$

almost isotropic (the 2*P term in the numerator) with a presumably small correction term in the denominator (presumably small, since we assumed Q << 1)

Lastly accept or reject based on the Rayleigh cross section; an energy independent efficiency of 66% (i.e., 2/3).

Incoherent Scattering

The angular distribution of incoherently scattered photons is a product of the scattering function and the Klein-Nishina formula,

$$sig(\cos) = SF(E,\cos) * KN(E,\cos) \qquad (29)$$

SF(E,cos) = the scattering function
KN(E,cos) = Klein-Nishina formula

$$= C * (A'/A)^2 * \left[A/A' + A'/A - 1 + \cos^2\right]$$
$$= C * (A'/A)^2 * \left[\left(1 + \cos^2\right) + (A/A' + A'/A - 2)\right] \qquad (30)$$
$$= C * (A'/A)^3 * \left[\left(1 + \cos^2\right) * (A/A') + (A/A') * (A/A' + A'/A - 2)\right]$$

A = photon incident energy in electron rest mass units

The energy of the scattered photon is,

$$A' = A / \left[1 + A * x\right], x = 1 - \cos \qquad (31)$$

Substituting for A' and canceling terms we find,

$$KN(E,\cos) = \frac{\left[1 + \cos^2\right]\left[1 + A * x\right] + \left[A * x\right]^2}{\left[1 + A * x\right]^3} \qquad (32)$$

$$= \frac{\left[2 - x * (2 - x)\right] * \left[1 + A * x\right] + \left[A * x\right]^2}{\left[1 + A * x\right]^3} \quad x = 1 - \cos$$

Note, at low energy as A approaches zero, the Klein-Nishina equation approaches Rayleigh scattering,

$$KN(E,\cos) \rightarrow \left[1+\cos^2\right] \tag{33}$$

and the the energy of the scattered photon approaches that of the incident photon, i.e., the energy loss approaches zero and incoherent scattering approaches coherent scattering.

As in the case of coherent scattering, we will use an analytical expression to represent the scattering function. For hydrogen we have the relationship,

$$SF(E,\cos)+FF(E,COS)^2=1 \tag{34}$$

Although this is strictly not valid for other elements it is often used as an approximation. However, this suggests using,

$$SF(E,\cos)=Z-FF \tag{35}$$

where FF' has the same functional form as our fit for the form factor squared,

$$FF=\sum_j Aj/\left[1+Bj*x\right]^N \tag{36}$$

For each element we will use the same value of N as previously defined for the form factor squared, and Aj and Bj will be treated as fitting parameters. Note Aj and Bj here need not be the same as those defined for coherent scattering, e.g., for coherent scattering the sum of the Aj is Z^2, whereas here it is Z. However, when rescaled for this difference, they are very similar as predicted by equations 34 and 35; for hydrogen they are virtually identical.

At low energy this approaches zero as E^2 in the forward direction and at high energies it approaches unity in the backward direction; indeed in almost all directions, except the extreme forward direction.

For the normally used definition of the scattering function, it varies from 0 at low energy to Z at high energy. Therefore the one constraint that we have is,

$$Z=\sum_j Aj \tag{37}$$

and we can write,

$$\begin{aligned} SF(E,COS) &= Z - \sum_j Aj / \left[1 + Bj * x\right]^N \Big\} \\ &= \sum_j \left\{Aj - Aj / \left[1 + Bj * x\right]^N \right\} \\ &= \sum_j Aj * \left\{\left[1 + Bj * x\right]^N - 1\right\} / \left[1 + Bj * x\right]^N \end{aligned} \tag{38}$$

The results are similar to those obtained for coherent scattering, in the sense that it has been found that in no case are more then three terms required to obtain excellent agreement between the the EPDLscattering functions and the fit. One term is adequate for Z = 1 or 2, where we only have one shell (K). Two terms are required for Z = 3 to 10, where we have two shells (K, L). Higher Z elements require an additional term. Incoherent scattering is usually described as an interaction between a photon and the outer most, most losely bound electrons. So what we seem to see is that the sum rather than including contributions from each subshell, saturates and only requires up to three terms to represent the contribution of the outer most subshells.

Figs. 3 and 4 illustrate comparisons between the original EPDL scattering functions and the fits that can be used in applications.

At low energies the scattering function plays an important role in suppressing forward scattering, compared to the Klein-Nishina formula. In the case of extreme low energies it essentially multiplies the Klein-Nishina formula by E^2. At higher energies the scattering function plays very little role, except at very forward angles where it will always suppress the forward scattering. At very high energies it plays essentially no role and is often simply ignored in applications.

This suggests using a rejection technique to first sample the Klein-Nishina formula and then accept or reject based on our fit. In this case we need not invert our fit (as was done in the case of coherent scattering), we merely first sample the Klein-Nishina formula to define x and then define the sum,

$$SF(E,\cos) = \sum_j Aj * \left\{1 - 1 / \left[1 + Bj * x\right]^N \right\} \tag{39}$$

and accept if the sum is greater than or equal to Z times a random number. The efficiency will vary from 1/3 at low energy to essentially1 (100% acceptance) at high energies.

Fluorescence

The Livermore Evaluation Atomic Data Library (EADL) contains data to describe the relaxation of atoms back to neutrality after they are ionized, regardless of what physical process ionized the atom, e.g., photoelectric, electron ionization, internal conversion, etc.

The data in EADL includes the radiative and non-radiative transitionprobabilities for each subshell of each element, for Z =1 through 100. Given that an atom has been ionized by some process that

has caused an electron to be ejected from an atom, leaving a "hole" in a given subshell, the EADL data can be used to calculate the complete radiative (fluorescence) and non-radiative (Auger and Coster-Kronig) spectrum of x-rays and electrons emitted as the atom relaxes back to neutrality [6].

For a K shell photoelectric event in uranium if fluorescence is not considered all of the energy of the photon is assumed to be deposited locally, at the point of the event. If fluorescence is considered, a portion of the approximately 116 keV binding energy of the ejected electron will be emitted as fluorescence x-rays. The portion emitted will be independent of the photons incident energy, i.e., every photoelectric event leads to an ionized atom that will then return to neutrality, independent of how it was ionized.

Figs. 5 and 6 illustrate that these spectra can be quite complex. In this case a single "hole" in the K shell of uranium statistically leads to the emission of 154 different energy x-rays and 2772 different energy electrons. Of course in any single given event far fewer x-rays and electrons are emitted, but when averaged over a large number of such events this will be the observed emitted spectra. The most important point to note is that rather than the entire energy being deposited locally, over 89% of the binding energy is re-emitted as fluorescence x-rays. These x-rays are emitted just below photoelectric edges, where the cross section can be quite small, which allows these x-rays to be quite penetrating. In absolute terms this means that a photoelectric event due to a photon just above the K edge at 116 keV will lead to the emission of about 100 keV off fluorescence x-rays - 89% of its energy; a 1 MeV photon will also result in about 100 keV of fluorescence x-rays - about 10% of its energy, etc. In the case of a 116 keV photon the local deposition will only be 16 keV. However, if fluorescence is not considered, it is assumed to be 116 keV; over 700% higher than the actual value. This over estimation will decrease at higher energies, but even by 1 MeV it will still be about 10% too high. From Fig. 6 we can see that most of the fluorescence x-ray energy will be emitted in a narrow band near 100 keV, just below the K edge where the cross section is only about 25% of the cross section at the top of the K edge, allowing these x-rays to be quite penetrating. For photon transport calculations extending down to energies below several MeV, to realistically model the transport, these fluorescence x-rays should be included in calculations.

This point has been recognized for many years and fluorescence has been included in modern Monte Carlo photon transport codes [7, 8]. In these codes the "jump" in the photoelectric cross sections across an edge is used to estimate the fluorescence yield for each subshell.

Now that the photoelectric subshell cross sections are available from EPDL and the fluorescence yield is available from EADL we can use a more detailed model for fluorescence. The subshell cross sections can be used to define what subshell was ionized, and once a subshell is selected our fluorescence yield data can be used to define the emitted x-rays. However, to be able to do this efficiently in calculations we must decide what is or is not important and try to include only those details that are important.

These spectra are judged to be too complicated to sample in detail in applications. However, the most important details can be efficiently sampled. We can use the fact that fluorescence decreases by roughly an order of magnitude for each successive shell. For example, in the case of uranium the fluorescence due to a K shell vacancy is almost 100%, whereas the L shell will be about 10%, the M shell about 1%, etc. In addition we can divide the photon spectrum into those x-rays due to

the initial vacancy being filled (what I will refer to as direct or primary x-rays) which are the most energetic x-rays emitted, and those x-rays due to vacancies generated in other shells as the atom relaxes back to neutrality (what I will refer to as secondary x-rays). I will refer to the combination of direct or primary and secondary as the enhanced or total yield.

Fig. 5 illustrates the emitted x-rays (fluorescence) due to a single vacancy in the K shell of uranium. The boxes represent the individual missions and the solid line represents the integral of the emitted energy spectrum. From this figure we can see that there are 154 individual x-rays emitted, but most of the emissions in terms of probability and energy are in two narrow energy bands just below the K and L edges; these two bands correspond to the direct and secondary fluorescence yields. Based on the integral of the spectrum, in this case the primary fluorescence just below the K edge accounts for about 95% and the secondary emission just below the L edge another 4.8%. The entire remainder of the spectrum accounts for only about 0.2% of the emitted x-ray energy, which is small compared to the uncertainty in the emitted spectrum. This suggests that for use in applications rather than attempting to model the entire emitted fluorescence x-ray spectrum all we need model are the two narrow bands of emission just below the K and L edges, in the case of a K shell vacancy; or L and M, for L vacancies; M and N, for M vacancies, etc.

Based on the EADL data, we can calculate [6] the direct and secondary fluorescence yields, both in terms of number of photons and energy emitted as fluorescence for every subshell of every atom (Z =1 through100). For use in calculations, this data has been reduced to a form where a vacancy in any subshell can result in the emission of up to two fluorescence x-rays where the emission probabilities and energies have been defined to exactly conserve the direct and enhanced fluorescence yields, both in terms of number and energy. These two x-rays per vacancy can accurately model the two narrow bands of emitted x-rays that we saw in the Fig. 5.

Since the fluorescence yield decreases rapidly with subshell, an accurate model of fluorescence yield does not require all of the individual subshells to be represented. For use in applications the photoelectric subshell cross sections have been grouped in: K, L1,L2, L3, M, N, O, P, Q, i.e., the most important inner subshells of K and L are represented separately, and the remaining subshellsof each shell are grouped together. Furthermore, fluorescence is only considered for K, L1, L2, L3, M and N, which tracks the yield down to a very low level, well below the uncertainty in our atomic relaxation data.

Following each photoelectric event we first use the subshell crosssections to randomly select an electron vacancy in a subshell. Once this has been done, the probability of fluorescence yield for that subshell is used to randomly emit x-rays of a given energy; up to two x-rays per primary vacancy are allowed. Even in the extreme case of high Z elements where the K shell fluorescence yield can approach 100%, the two x-rays allowed in this model will track the yield from K shell vacancies down to about 1%. By allowing individual subshells to be sampled the fluorescence will be tracked down ever further in energy, e.g., if we had statistically sampled a vacancy in an L subshell the yields could approach about 10%and 1%, tracking the yield down to about 0.1%.

Pair and Triplet Production

In the case of pair production, the photon interacts with the field of an entire atom. The photon disappears and an electron-positron pair is created. The sum of the energies of the electron-positronpair is the incident energy of the photon minus the rest mass of the electron-positron pair.

In the case of triplet production the photon interacts with the field of an electron. The photon disappears and an electron-positron pair is created, and an electron is ejected from the atom (leaving an ionized atom). The sum of the energies of the electron-positron pair plus the ejected electron is the incident energy of the photon minus the rest mass of the electron-positron pair and the binding energy of the ejected electron. Compared to the energies of the electron-positron pair, generally the energy of the ejected electron is quite small

Pair and triplet production are fairly complicated processes, since they are three body processes. For example, in pair production the electron and positron need not equally share the available kinetic energy; indeed at higher energies the spectrum for both becomes quite wide. Here I will merely mention that this spread in the spectra will effect bremsstrahlung emitted by the electron and positron as they slow down in the medium.

Here I will use the simplest possible model for pair and triplet production. I will assume that the electron and positron both slow down and come to rest close to the point of the pair or triplet production event. Therefore, all of their kinetic energy will be deposited locally, and when the positron annihilates two 0.511 MeV photons are created at the point of the pair or triplet event. In the case of triplet production, I will also ignore the low energy ejected electron and the ionized atom.

Later in this paper, I will again discuss pair and triplet under the section What's Next?

The Importance of Each Process

Fig, 7 illustrates the photon cross sections for four elements spaced across the periodic table. In all cases the variation of the cross sections are smooth functions of Z, so that even from merely these four examples we can see all of the trends of the various cross sections. This figure was produced interactively using Epicshow; the top of the figure shows the Epicshow mouse driven interactive user interface.

Generally, at low energy photoelectric is by far the dominant process. In comparison, the coherent and incoherent cross sections are so much smaller, that they are of importance only in special calculations, such as back scattering measurements, where their cross sections may be small, but these are the only processes available to back scatter photons. As described above, at low energy incoherent scattering approaches coherent scattering (no energyloss) and photoelectric is the only effective energy loss process for photons.

At low energies, in high Z elements, fluorescence can be a very important effect, since it can effectively transfer photons from energies above photoelectric edges, where the cross section is high, to energies just below the edges, where the cross section can be much smaller; thereby,

allowing these photons to be much more penetrating. Since at low energies the photoelectric cross section can be very large, fluorescence can appear almost to be a surface effect, i.e., most of the photoelectric events above the edges will occur very close to the surface of a high Z element. This will tend to increase the reflection from high Z elements. However, it can also contribute to penetration through materials. For example, in high Z elements the cross section at the bottom of the K edge is about 1/4 to 1/5 that of the cross section at the top of the edge. Therefore, if we have a material that based on the cross section at the top of the K edge is say 10 mean free paths thick (we expect little if any transmission), fluorescence can move photons to below the K edge where the cross section is only 2 to 2.5 mean free paths thick.

At high energies pair and triplet production become the dominant processes. Above about 10 MeV their cross sections are so much larger than the coherent and photoelectric cross sections that the latter can be effectively ignored. Even at fairly high energies incoherent scattering continues to play an important role and should not be ignored. At these high energies coherentand incoherent scattering are very forward peaked, and cause very little back scatter.

At intermediate energies between the high keV and low MeV regions incoherent scattering can be very important. In this energy range the photoelectric cross section has decreased to a small value and the pair and triplet production cross sections have not yet become significant. Therefore, the only effective process that can decrease the energy of photons is incoherent scattering. From Fig. 7 we can see that incoherent scattering in this energy range is particularly important for low Z elements, e.g., hydrogen. At lower energies the incoherent cross section approaches zeroas E^2, and becomes dominated by the rapidly increasing photo-electric. Similarly, at higher energies the incoherent cross section decreases, and eventually becomes dominated by the rapidly increasing pair and triplet production cross sections.

Coherent scattering can be an important process in the keV region, in that by scattering photons it will tend to keep them from escaping from a medium, but in no case is coherent scattering the dominant process. At lower energies the coherent cross section approaches zero as E^2, and at higher energies it also decreases toward zero. Just below photoelectric edges in high Z elements the coherent cross section can be a significant contribution to the total cross section, e.g., about 10%, that does effect transport.

Example Results

All of the data discussed above is now available in a simple tabulated format, to allow the data to be easily moved between computers. On any given computer it is then converted to binary, random access files for use in applications.

This data can be examined using the program Epicshow [9] and actual photon Monte Carlo transport calculations can be performed using the program Epicp [10].

Epicp is designed as a test bed program to develop optimum algorithms for handling photons, for later use in Epic (Electron Photon Interaction Code). Epicp uses all of the data described in this report, and allows various models to be turned on or off, to determine the importance of each model. For example, coherent and incoherent scattering can be modeled either with or without

form factors and scattering functions. Photoelectric events can be modeled with or without fluorescence emission. Cross sections can be modeled using the energies at which they are tabulated in the data bases (most accurate) or using the same fixed energy grid for all elements (fastest). By comparing the results and running time using different models we can easily determine how accurate any given model is and how expensive it is to use.

Below, I present results to illustrate the use of this data and I also present conclusions that can be reached from these results. In all cases I will use a simple geometry, so that we can easily interpret the results. I will use cylindrical geometry to simulate a detector, and I will calculate: 1) deposition within the detector, 2) transmission through the detector, 3) reflection from the detector, and 4) lateral leakage from the detector. Both analogue and expectation results will be presented; having both types of results available allows a simple check that as long as many histories are considered both converge to the same answer. All results are presented in 500 equally spaced energy bins. No attempt has been made to fold the results with a detector response function; the results presented are exactly as calculated, and therefore differ from what one would actually measure with a real detector. This has been done intentionally in order to emphasize the effects that will be discussed below.

High Energy Application

The first application is a monoenergetic 4.43 MeV photon incident on a NaI detector 7.62 cm in diameter and 7.62 cm in depth. This example is intended merely to introduce the idea of detector deposition and to point out one approximation that should be avoided.

Fig. 8 presents Epicp results for this problem. The transmission, reflection and lateral leakage are in units of photons per MeV for each contributing individual event. In the case of deposition, for each incident photon the total amount of energy deposited is scored as a single event. If all of the energy of all incident photons is deposited the result would be non-zero only at 4.43 MeV. Instead we see a typical response function. Note, the peaks about 1 and 0.5 MeV below 4.43 MeV. These correspond to the build up and escape from the detector of both or one of the 0.511 MeV photons created by positron annihilation. The results have not been folded with the detector response in order to more clear see and understand these two peaks: in an actual detector response these peaks are much wider. The transmission, reflection, and lateral leakage all show peaks due to the leakage of 0.5 MeV photons. We do not expect a peak near 1 MeV, since even if both 0.5 MeV photons leak they are scored as two separate 0.5 MeV photons.

One might think that in this case the calculation could be sped up by assuming that rather than each pair production event leading to two separate 0.511 MeV photons, we could assume that we will run enough photons histories that we could assume that each pair production events produces only one 0.511 MeV photon, of weight 2; the large number of photon histories could then be relied on supply enough events to adequately describe the position and direction of all such photons. This assumption actually works quite well to describe the transmission, reflection, and lateral leakage, but not the deposition. In order to reproduce the two peaks in the deposition one must track each of the photons separately, otherwise you can never have the case where only one of them escapes, leading to the peak about 0.5 MeV below the source energy.

Fixed or Variable Cross Section Energies

There are a number of Monte Carlo codes [7, 8] that use a fixed set of energies to represent all photon cross sections for all elements. This simplifies the codes and speeds up the calculation, e.g., for a photon of a given energy, once you have defined the energy interval in the cross section, tables this can be used to define the cross sections for all materials in all zones.

This approach requires that certain compromises be accepted between speed and accuracy. For example, the energy of the K edge of each element is to a good approximation a simple logarithmic function of atomic number, varying from about 14 eV for hydrogen (Z = 1), to about 140 keV in fermium (Z = 100). Without using an excessive number of tabulated energy points over this energy range, it would be difficult to accurately approximate the K edge for all elements. If we consider not only the K edge, but all other edges, plus the additional general problem of accurately interpolating in energy between tabulated values, we must conclude that if we wish to use the same energies for all elements we will have to somehow compromise the accuracy of the photon cross sections. Is this important?

This effect will only be important at energies near K edges, i.e., in the worse case below about 150 keV. For higher energy applications, there is no problem in using the same energy points for all elements; the only point to be concerned with is properly modeling the onset of pair production at its 1.022 MeV threshold and triplet production at its 2.044 MeV threshold. Therefore, the following discussion is only of interest to those readers involved in lower energy applications.

What we will examine here is: 1) how accurate is this procedure, 2) how much faster is it than representing the cross sections for each element using a different set of tabulated energies for each element, 3) what are the real advantages of one approach versus the other.

In an attempt to answer these questions, we will use the 176 energy points used by the TART code to represent all cross sections and first see what effect this has on both the position of the K edge and the magnitude of the cross section near the K edge. The Epic cross sections try to model each photoelectric edge as a discontinuity with repeated energy points at the bottom and top of each edge. TART represents it with the two nearest fixed energy points on either side of the real edge energy. How accurate is this? We will use exactly the procedure used to make the photon data library used by TART, 1) interpolate the actual photon cross sections to the 176 energies and define the value strictly based on interpolation (no attempt is conserve integrals or anything else), 2) I will then define the "TART position of the K edge" bottom and top as the first energy at or below the actual K edge and the first energy at or above the actual K edge, 3) we can then compare the value of the cross sections at these points to the actual values in EPDL.

Fig. 9 presents results for the entire period table, from Z = 5 through 100 (TART only extends down to 100 eV and as such does not include the K edge of the lowest Z elements). First the figure shows a comparison of the energy of the EPDL K edge to the TART K edge top and bottom energies. What we see, is that using the TART 176 energy points can shift the energy of the top and bottom of the K edge by about 10% for a number of elements. The figure next compares the value of the cross section at the bottom and top of the K edge for EPDL and TART. What we see is that using the TART 176 energy points can increase the bottom cross section by up to about 30%

and decrease the top cross section by up to 30% for a number of elements. Lastly, the figure shows the values at both top and bottom of the K edges. From this figure we can see that the changes in the cross section due to using the TART 176 points tend to move the top and bottom values up and down together; fortunately, we do not have any cases where 30% changes move in opposite directions, thereby, changing the jump ratio across the K edge by even more.

In order to determine whether or not these changes are important, we can now use the above results to select some worses cases from the entire periodic table and see what happens in an actual transport calculation.

Based on the changes in the position and magnitude of the cross sections, when using a fixed energy grid, one might expect to see rather large differences in the results using one method or the other. By using a large number of Epicp and TART runs focussed on where we expect to see large differences, the results indicate surprisely little difference in the results. As long as a problem involves a broad spectrum of photons, the energy intervals over which the cross sections are modified near the K edges is small compared to the entire energy range of interest and results in very little change in overall answers.

However, if the focus of the application is effects near the K, or other edges, then one can see rather large differences in the results. For example, obviously, if you decrease the photoelectric by 30% you expect a decrease in deposition by 30%, but only over the narrow energy range where the cross section was deceased. If this is the energy range of interest to you, this is an important effect. A second effect to consider, is that in shifting the K edges by up to 10%, it may no longer be possibleto use transmission measurements defining the position and strength of K edges to define the composition of a material containing neighboring or near Z elements.

Fig. 10 compares the fluorescence yield as a fraction of the incident photon energy using the original tabulated energies (as read from the data base), 176 and 401 fixed energy points. If you only consider a wide energy range, using fixed energies will have little effect on integral values (top of figure). For this particular problem of transport through Z = 90 (where we expect large differences) there is no significant difference in the integral deposit, transmission, reflection or lateral leakage; differences occur over such a small portion of the total energy range that the effect on integral values is simply not significant. However, if you are interested in very narrow energy ranges, particularly near edges, using fixed energies can have a significant effect (bottom of figure). In this case the fluorescence yield and therefore deposition are obviously effected, but it is also difficult to see the K edge, which makes it difficult to determine the composition of this material. Is this an important effect in your applications? Only you can answer this question.

In terms of running time, there is a definite advantage to using fixed energies. For simple problems only involving a few materials and zones, there isn't that much difference between them. However, as problems become complex and involve more and more materials and zones, using fixed energies results in significantly less running time. In the latter case, a mixture of material decreases the importance of changes across edges, further justifying the use of fixed energies.

In terms of simplicity of the codes, there is a definite advantage to using a fixed energy grid, e.g., in complicated geometries defining the cross section when a photon enters each spatial region is much simpler using a fixed energy grid.

In summary, based on the above results, it appears that each approach can be used to good advantage in different applications, and it is not possible to make one sweeping general recommendation that one approach is "better" than the other. If you are willing to invest the time to handle different energies for each element you can be sure that your code will be quite general and need not worry about the special situations described above; be aware, you will pay a penalty in running time for complicated problems. However, if you already have a code that uses fixed energies and do not want to invest the time to upgrade it, for most calculations involving broad spectra of photons and only considering integral response over wide energy range, fixed energies are adequate to obtain accurate answers.

Epic tries to accommodate both approaches. In the Epic data base each element is tabulated using energies that have been selected to best represent the data. For use in application the user has the option to perform calculations using the data exactly as represented in the data base (most accurate), or using the same, fixed energy grid for all elements (fastest). Conversion to the latter form as the data is read from the data base for use in calculations is trivial and does not add any significant overhead to calculations. As an improvement over the TART 176 point between 100 eV and 30 MeV, Epic uses 401 points between 10 eV and 1 GeV, with 50 points logarithmically equally spaced in each energy decade; this completely uniform spacing from 10 eV to 1 GeV allows the energy interval for cross section lookup to be defined using a single line of FORTRAN coding. Similar to the above results for TART (Fig. 9), Fig. 11 shows results for this 401 fixed point energy grid. From this figure we can see that the 401 points results in shifts of K edge energies by up to 4% (compared to 10% for TART), and changes in the cross section by up to 10% (compared to 30% for TART). With this approach users can select whatever scheme is most appropriate for their calculations, i.e., either accuracy or speed.

Fluorescence

Fluorescence yield is a function of atomic number (Z). For the K shell it varies from close to 100% for fermium (Z = 100) to essentially 0% for hydrogen (Z = 1). It is also a function of shell, decreasing by roughly a factor of 10 for each successive shell, e.g., from close to 100% for K, about 10% for L, etc. It is also a function of energy, being important only close to photoelectric edges. Therefore, we need not be concerned with low Z elements, or high energy applications, well above the K edges of all materials involved. However, we should look at high Z elements for lower energy applications, i.e., below a few MeV.

The following example illustrates the effect of fluorescence. In this case Epicp was used to calculate the deposition within a cylinder of lead with and without fluorescence included in the calculation. Figs. 12 and 13 illustrate the expected energy deposition in the lead due to a single photoelectric event. As we can easily see, not including fluorescence will over estimate the energy deposition, particularly above the K edge. From the Fig. 12, using log energy scaling, the effect may not look too severe, since it appears to only be restricted to a small portion of the plot.

However, from Fig. 13, using linear energy scaling, we can see that in fact the effect is significant over most of the energy range.

In this example, each K shell photoelectric event leads to the emission of about 80 keV of fluorescence x-rays. The effect is most obvious near the K edge and decreases as a fraction of incident photon energy at higher energies, e.g., by 1 MeV it is about an 8% effect.

So if it wasn't deposited in the first photoelectric event, where did the energy go? In order to find out, we have to look at the total deposition, transmission, reflection and lateral leakage; by conservation, the sum of these quantities must in all cases be equal to the energy of the incident photon (it has to go someplace). For the case considered here, with no fluorescence almost all of the energy is either deposited or transmitted through the cylinder: 75% deposited, 24.4% transmitted and about 0.6% reflected or lateral leakage. Of the deposition 74.6% is due to photoelectric and only 0.4%to Compton (incoherent) scattering. With fluorescence the deposit is decreased to 62%, 28% is transmitted, and 10% reflected or lateral leakage. As pointed out above, at low energies the photoelectric cross section is so large that fluorescence is almost a surface effect. In this case the many photoelectric events close to the surface causes a rather large increase in reflection and a somewhat smaller increase in the transmission.

Figs. 14 through 17 show the reflection and deposition with and without fluorescence. The fluorescence x-rays are emitted just below the K and L edges, which can be clearly seen on the following plot of the reflection (Figs. 14 and 15). In the case of the deposition, (Figs. 16 and 17) these x-rays undergo further photoelectric and Compton events, leading to the large increase in the deposition over the energy range 12 to 70 keV, below the K edge and a smaller increase below 12 keV, below the L edge.

Without fluorescence, each photoelectric event causes a photon to deposit all of its energy and the photon "disappears." With fluorescence secondary x-rays are emitted, that in turn must be transported. Therefore, inclusion of fluorescence x-rays will increase running time, due to tracking these secondary x-rays.

In summary, for applications involving high Z elements, below a few MeV, it is important to include the effect of fluorescence in order to obtain realistic calculational results. At higher energies the photoelectric cross section is so small that the probability of a photoelectric event, and therefore, fluorescence is very small. Therefore, it isn't necessary to build into codes a rule of thumb to ignore fluorescence above some incident photonenergy; its happens naturally based on the cross sections.

Coherent and Incoherent Scattering

Fig. 18 summarizes the effect of anomalous scattering on the coherent cross section. This effect is important at low energies and extends up to several times the K edge energy, i.e., about 1 MeV in high Z elements. Without anomalous scattering, the coherent scattering approaches a constant value at low energy. With anomalous scattering it approaches the correct zero limit as E^2 at low energy. In uranium the difference at 10 eV is about 5600 barns without anomalous scattering and

10 barns with it (a factor of 560 difference). Near photoelectric edges, anomalous scattering causes a significant decrease in the coherent cross sections, which leads to lowering of the cross sections just below the edges, allowing increased transport of photons. Since the effect of anomalous scattering has been included in the Epic coherent cross sections, we need not explicitly consider the effect further in applications, i.e., the effect is automatically included.

Fig. 19 summarizes the effect of the scattering function on the incoherent cross section. This effect is important at low energies and extends up to several hundred keV in high Z elements. Without the scattering function the incoherent cross section, defined by integrating the Klein-Nishina formula, approaches a constant value at low energy. With the scattering function it approaches the correct zero limit as E^2 at low energy. At lower energies where both coherent and incoherent cross sections are approaching zero as E^2, obviously including the effects of anomalous scattering and the scattering function, greatly reduces total scattering. Since the effect of the scattering function on the incoherent cross section has been included in the Epic incoherent cross sections, we need not explicitly consider the effect further. However, we do have to consider the effect on scattering angle and energy loss.

Figs. 20 and 21 illustrate the effect of the scattering function on the average incoherent scattering σ (1 - cos), and energy loss. Since the scattering function suppresses scattering in the forward direction, at lower energies the effect of the scattering function is to increase both the average 1 - cos and energy loss. By roughly 0.1*Z MeV (100 keV in hydrogen, 10 MeV in fermium) and higher energies, the scattering function has no appreciable effect on either the average 1 - cos or energy loss, and is often simply ignored in calculations

Fig. 22 illustrates the effectiveness of incoherent scattering as an energy loss process. At high energies it is a very effective process for energy loss, since a single collision can result in a photon losing a significant fraction of its energy. At lower energies it becomes progressively less effective. Since the energy of an incoherently scattering photon is,

$A' = A / [1 + A * x]$, $x = 1 - \cos$

A = *photon incident energy in electron rest mass units.*

the maximum energy loss per collision is roughly: 1 keV ~ 0.4%, 10 keV ~ 4%, 100 keV ~ 28%, 1 MeV ~ 80%. As pointed out above, at lower energies the Klein-Nishina formula approaches Rayleigh scattering, the energy loss approaches zero, and as such incoherent and coherent scattering both approach the same form. Fig. 21 illustrates that at low energy the average energy loss without including the scattering function decreases to about 70% of the energy loss with the scattering function. But from Fig. 22, we can see that in no case does the scattering function, play a significant role in changing the fractional energy loss.

It is easy enough to illustrate the difference in the angular distribution for coherent or incoherent scattering, and the energy spectrum for incoherent scattering, with or without using form factors and scattering functions. If we consider monoenergetic photons the calculations of angular and

energy distributions doesn't require Monte Carlo; it is an analytical calculation. The variation of the scattering function is a very smooth function of Z, the effect extending to higher and higher energies with increasing Z. Therefore, the worst case to consider is Z=100 (fermium). Figs. 23 through 25 illustrate Monte Carlo results (used by Epicp to test the actual sampling of the distributions) with and without the scattering function, at 10 keV, 100 keV and 1 MeV. In all cases the effect of the scattering function is to suppress the high energy spectrum and forward scattering; since these are normalized distributions, they must cross one another at some point, so that it also increases the low energy spectrum and backward scattering. At 10 keV we can easily see the difference; at this energy without the scattering function the angular distribution is essentially merely $1 + \cos^2$ (the same as Rayleigh scattering). At 100 keV the distribution is more forward peaked, and we can still see the difference. By 1 MeV the distributions are essentially identical, except for a very small range in the forward direction of the angular distribution and high energy limit of the spectrum. There is no reason to present higher energy results, since we expect the scattering function to have essentially no effect at higher energies.

It is easy to present results such as these for single energies. However, it is much harder to define actual applications where these effects are important in an integral sense. As pointed out above, coherent scattering is never the dominant process, and where incoherent scattering is dominant tends to be in the high keV region of low Z elements, where the scattering function has little effect. The net effect is that when we examine real transport situations, where all processings are occurring, the effect on integral parameters, such as deposition, transmission, reflection, etc., is much less than one might expect based on examining angular and energy distributions with and without form factors and scattering functions.

At higher energies, the form factor will make coherent scattering more forward peaked, which tends to make photons transport further in their direction of travel. In an integral sense this effect can be seen, since it will tend to increase transmission, and decrease reflection. However, since coherent is never the dominant process the effect is small.

At lower energies the scattering function will make incoherent scattering more backward peaked, which tends to make photons transport less in their direction of travel. In an integral sense this effect can be seen, since it will tend to decrease transmission and increase reflection. However, at lower energies the photoelectric cross section is so large that the effect on transmission is quite small, but the effect on reflection can be significant, e.g., for back scattering measurements at low energies it is important to include the effect of the scattering function.

In summary, for general transport calculations do not expect to see dramatic effects with or without form factors and scattering functions. However, in special applications, particularly back scattering measurements, the effect can dominate the answers.

Multi-Group Calculations

Above I have only discussed Monte Carlo, but it is worth noting that the Epic photon data base can also be used in multi-group calculations. The tabulated linearly interpolable cross sections are easier to use than the ENDF/B-VI formatted data to define multi-group averages. The analytical forms for coherent and incoherent scattering and fluorescence can be easily used to define group to

group transfer matrices. In the case of scattering, the results should be identical to those obtained using theENDF/B-VI data. In the case of fluorescence, Epic contains more detail than allowed in the ENDF/B-VI formats.

What's next?

In this paper, I have really only looked at one portion of the picture of photon transport. For example, if a 20 MeV photon undergoes a pair production event, the simplest assumption is that eventually the positron will come to rest and annihilate, creating two 0.511 MeV photons. But we should ask: of the initial 20 MeV we got back about 1 MeV of energy in the form of our two 0.511 MeV photons. What happened to the other 19MeV? Similarly, if a 20 MeV photon undergoes an incoherent scatter it can lose up to almost 99% of its energy. We can continue tracking the scattered photon, but what happened to the 99% of the energy?

The most common assumption used in many photon transport codes is that any energy lost by the photons is deposited locally at the point where each event takes place. In fact, none of the processes that I have discussed in this paper allow photons to directly deposit energy; all that photons can do is transfer their energy to electrons and positrons. So that the proper way to answer the questions that I asked above is to consider what happens to the electrons and positrons that receive energy from photons. In the case of a 20 MeV pair production, do the electron and positron really stop and deposit all of their energy very close to where the pair production occurred, or do they travel and maybe even escape from the medium? The same should be asked of electrons that receive energy from incoherent scattering events. What about feedback? Is it important to consider bremsstrahlung, that will create more photons? Or electron ionization, that can lead to fluorescence?

I am not going to even try and cover this topic here. That's what I will cover next: A Simple Model of Electron Transport.

Conclusions

In this paper I described a simple model of photon transport. This simple model includes: tabulated cross sections and average expected energy losses for all elements between hydrogen (Z = 1) and fermium (Z = 100) over the energy range 10 eV to 1 GeV, simple models to analytically describe coherent and incoherent scattering, and a simple model to describe fluorescence. This is all of the data that is required to perform photon transport calculations.

Each of these simple models was first described in detail. Then example results are presented to illustrate the accuracy and importance of each model.

These models have now been implemented in the Epic (Electron Photon Interaction Code). All of the figures and results presented here are from Epicshow, an interactive program to allow access to the Epic data bases, and Epicp, a simple photon transport code designed to develop optimum algorithms for later use in Epic. All of the data described in this paper and all of the programs needed to use it, are available from the author.

Throughout the paper, I have tried to define where various models are important: fluorescence and scattering function at low energy, form factor at high energy. I have also tried to define guidelines as to where various models can often been ignored, e.g., the scattering function above 0.1*Z MeV. Here, I will present a somewhat different viewpoint. Where these models are unimportant, the events that use them are highly unlikely. For example, at high energy the photoelectric cross section is so much lower than the other cross sections, that the probability of a photoelectric event is highly unlikely; therefore, so is fluorescence. The same is true at high energy for coherent scattering. Since these events are highly unlikely, whether they are treated exactly or using an approximation will not have a significant effect on running time. When a fixed energy grid is used it is adequate for most applications, and can decrease running time for complicated problems, but it may or may not give accurate answers for any specific application.

Photons are quite different from neutrons, electrons, positrons and charged particles, in that in all elements, at all energies, the expected energy loss due to even one event is a significant fraction of the photons energy. So that photons do not have many collisions or events before they "disappear." Unlike other particles that undergo many events, each of which may have little effect on the overall history of the particles, for photons each and every event can have a major impact on a history. Therefore, care has to be used to model each and every event as accurately as possible if we are to expect accurate answers in as many different applications as possible.

The bottom line is: can you afford to have a transport code that works for most applications - but may not work for the specific applications that you are interested in. Using a fixed energy grid can reduce running, but most other approximations discussed here have little effect on running time, but may prevent the code from giving accurate answers in certain applications - certain applications that the user will not be able to predict in advance nor be able to recognize the answers to be inaccurate. When we look at efficiency and even running time the real bottom, bottom line is Howerton's first theorem: "We are in no rush for the wronganswer" [11].

Acknowledgements

Work performed under the auspices of the U.S. Department of Energy by the Lawrence Livermore National Laboratory under contract number W-7405-ENG-48

I thank S.T. Perkins (Lawrence Livermore National Laboratory) and J. Stepanek (Scherrer Institute) for their assistance and many helpful suggestions during the development of Epicp and Epicshow. I also thank Colleen Camacho (Lawrence Livermore National Laboratory) for typing the final form of this paper.

References

1. "Tables of Graphs of Photon-Interaction Cross Sections from 10 eV to 100 GeV Derived from the LLNL Evaluated Photon Data Library (EPDL), Parts A & B," by D.E. Cullen, et al., UCRL-50400, Vol. 6, Rev. 4, Oct 31, 1989, Lawrence Livermore National Laboratory.

2. "ENDF-6 Formats Manual," by P.F. Rose and C.L. Dunford, ENDF-102, Brookhaven National Laboratory.

3. "The 1989 Livermore Evaluated Photon Data Library (EPDL)," by D.E. Cullen, S.T. Perkins and J.A. Rathkopf, UCRL-ID-103424, March 1990, Lawrence Livermore National Laboratory.

4. "Elastic Scattering of Gamma-Rays and X-Rays by Atoms," by P.P. Kane, et al., Review Section of Physics Letters, 140, No. 2 (1986). North-Holland, Amsterdam.

5. "Atomic Form Factors, Incoherent Scattering Functions, and Photon Scattering Cross Sections," by J.H. Hubbell, et al, J. Phys. Chem. Ref. Data, 6, (1977).

6. "Program RELAX: A Code Designed to Calculate Atomic Relaxation Spectra of X-Rays and Electrons," by D.E. Cullen, UCRL-ID-110438, March, 1992, Lawrence Livermore National Laboratory.

7. 17026, Rev. 3, January 1990, Lawrence Livermore National Laboratory.

8. "MCNP - A General Monte Carlo Code for Neutron and Photon Transport, Version 3A," by J.F. Briesmeister, editor, LA-7396-M, Rev 2, September 1986, Los Alamos National Laboratory.

9. "Program Epicshow: A Computer Code to Allow Interactive Viewing of the EPIC Data Libraries, Version 94-1," by D.E. Cullen,UCRL-ID-116819, February 1994, Lawrence Livermore National Laboratory.

10. Program EPICP: A Computer Code to perform Photon transport "Monte Carlo calculations to Develop Optimized Algorithms," by D.E. Cullen (to be published).

11. Private Communication, R.J. Howerton (1973)

Table Captions

Example Epic Tabulated Photon Data

Figure Captions

1) Comparison of EPDL and Fit Form Factor
2) Comparison of EPDL and Fit Form Factor
3) Comparison of EPDL and Fit Scattering Function
4) Comparison of EPDL and Fit Scattering Function
5) Radiative (x-ray) Emission Spectrum
6) Non-radiative (electron) Emission Spectrum
7) Example Photon Cross Sections
8) Example Epicp Monte Carlo transport results
9) Comparison of EPDL and TART K edge parameters
10) Comparison of Fluorescence Yields
11) Comparison of EPDL and 401 point K edge parameters
12) Comparison of Energy Deposition with and without Fluorescence
13) Comparison of Energy Deposition with and without Fluorescence
14) Comparison of Reflection with and without Fluorescence
15) Comparison of Reflection with and without Fluorescence
16) Comparison of Energy Deposition with and without Fluorescence
17) Comparison of Energy Deposition with and without Fluorescence
18) Effect of Anomalous Scattering on the Coherent Cross Section
19) Effect of Scattering Function on the Incoherent Cross Section
20) Effect of Scattering Function on Average Scattering Cosine
21) Effect of Scattering Function on Average Energy Loss
22) Effect of Scattering Function on Average Energy Loss
23) 10 keV Incoherent Scattering with and without Scattering Function
24) 100 keV Incoherent Scattering with and without Scattering Function
25) 1 MeV Incoherent Scattering with and without Scattering Function

82	243	2.0719+02	1.1350+01	82-Pb-Nat					
MeV	Total	Photo.	Coherent	Incoher.	Pair	Triplet	Photo-DE	Incoh-DE	Pair-DE
1.0000-05	1.4702+07	1.4702+07	5.7651+00	1.5580-04			1.0000-05	2.7402-10	
1.2500-05	8.9032+06	8.9032+06	3.5860+00	2.4347-04			1.2500-05	1.0275-09	
1.5050-05	5.5635+06	5.5635+06	3.0188+01	3.5432-04			1.5050-05	1.7961-09	
1.5050-05	8.6140+06	8.6140+06	3.0188+01	3.5432-04			1.5050-05	1.7961-09	
1.6000-05	6.9746+06	6.9745+06	2.5819+01	3.9896-04			1.6000-05	2.0825-09	
2.0000-05	3.3958+06	3.3958+06	9.0781+00	6.2347-04			2.0000-05	3.2881-09	
2.5000-05	1.6853+06	1.6853+06	2.0633+00	9.7432-04			2.5000-05	4.7952-09	
2.6030-05	1.4983+06	1.4983+06	3.6550+00	1.0599-03			2.6030-05	5.1057-09	
2.6030-05	5.1829+06	5.1829+06	3.6550+00	1.0599-03			2.6030-05	5.1057-09	
2.8810-05	6.1801+06	6.1801+06	1.0208+01	1.2967-03			2.8810-05	5.9436-09	
2.8810-05	8.1267+06	8.1267+06	1.0208+01	1.2967-03			2.8810-05	5.9436-09	
3.2000-05	1.3278+07	1.3278+07	2.8643+01	1.5966-03			3.2000-05	6.9051-09	
4.0000-05	4.4100+07	4.4100+07	1.9015+02	2.4950-03			4.0000-05	9.3164-09	
5.0000-05	4.4341+07	4.4341+07	3.0861+02	3.8991-03			5.0000-05	1.2330-08	
6.3000-05	2.2431+07	2.2431+07	2.6018+02	6.1911-03			6.3000-05	1.6249-08	
8.0000-05	9.1335+06	9.1334+06	1.6883+02	9.9847-03			8.0000-05	2.1373-08	
8.7640-05	6.2375+06	6.2374+06	1.0592+02	1.2005-02			8.7640-05	2.3676-08	
8.7640-05	7.3704+06	7.3703+06	1.0592+02	1.2005-02			8.7640-05	2.3676-08	
1.0000-04	4.5024+06	4.5023+06	1.5956+02	1.5603-02			1.0000-04	2.7401-08	
1.1091-04	2.9540+06	2.9538+06	1.2235+02	1.9163-02			1.1091-04	3.8528-08	
1.1091-04	3.5695+06	3.5694+06	1.2235+02	1.9163-02			1.1091-04	3.8528-08	
1.2500-04	2.2422+06	2.2421+06	1.6672+02	2.4255-02			1.2500-04	5.2897-08	
1.4781-04	1.2168+06	1.2167+06	1.3976+02	3.3899-02			1.4781-04	7.6160-08	
1.4781-04	1.3559+06	1.3558+06	1.3976+02	3.3899-02			1.4781-04	7.6160-08	
1.5283-04	1.2904+06	1.2903+06	1.3222+02	3.6211-02			1.5283-04	8.1279-08	
1.5283-04	1.3495+06	1.3494+06	1.3222+02	3.6211-02			1.5283-04	8.1279-08	
1.5304-04	1.3455+06	1.3453+06	1.3226+02	3.6308-02			1.5304-04	8.1493-08	
1.5304-04	1.4518+06	1.4517+06	1.3226+02	3.6308-02			1.5304-04	8.1493-08	
1.6000-04	1.4022+06	1.4021+06	1.3201+02	3.9513-02			1.6000-04	8.8591-08	
2.0000-04	1.2509+06	1.2508+06	1.0351+02	6.1421-02			2.0000-04	1.2939-07	
2.5000-04	2.3099+06	2.3098+06	8.1066+01	9.5475-02			2.4999-04	1.8038-07	
3.2000-04	5.2457+06	5.2455+06	2.3151+02	1.5452-01			3.1999-04	2.9286-07	
4.0000-04	5.1061+06	5.1058+06	3.6998+02	2.3796-01			3.9999-04	4.4566-07	
4.1249-04	5.0113+06	5.0109+06	3.8864+02	2.5280-01			4.1248-04	4.6952-07	
4.1249-04	5.1224+06	5.1220+06	3.8864+02	2.5280-01			4.1248-04	4.6952-07	
4.3523-04	5.0475+06	5.0470+06	4.5458+02	2.8049-01			4.3522-04	5.1912-07	
4.3523-04	5.1364+06	5.1359+06	4.5458+02	2.8049-01			4.3522-04	5.1912-07	
5.0000-04	4.6457+06	4.6451+06	5.9635+02	3.6299-01			4.9999-04	6.9395-07	
6.3000-04	3.4769+06	3.4762+06	7.2803+02	5.5594-01			6.2999-04	1.0898-06	
6.3430-04	3.4464+06	3.4457+06	7.5701+02	5.6300-01			6.3429-04	1.1052-06	
6.3430-04	3.6504+06	3.6497+06	7.5701+02	5.6300-01			6.3428-04	1.1052-06	
7.5602-04	2.8225+06	2.8215+06	1.0123+03	7.7119-01			7.5600-04	1.5412-06	
7.5602-04	2.8604+06	2.8594+06	1.0123+03	7.7119-01			7.5600-04	1.5412-06	
8.0000-04	2.5820+06	2.5809+06	1.0757+03	8.4848-01			7.9998-04	1.7384-06	
8.7672-04	2.2211+06	2.2200+06	1.1320+03	9.9094-01			8.7670-04	2.0911-06	
8.7672-04	2.2641+06	2.2630+06	1.1320+03	9.9094-01			8.7670-04	2.0911-06	
1.0000-03	1.7871+06	1.7858+06	1.2907+03	1.2354+00			9.9997-04	2.6578-06	

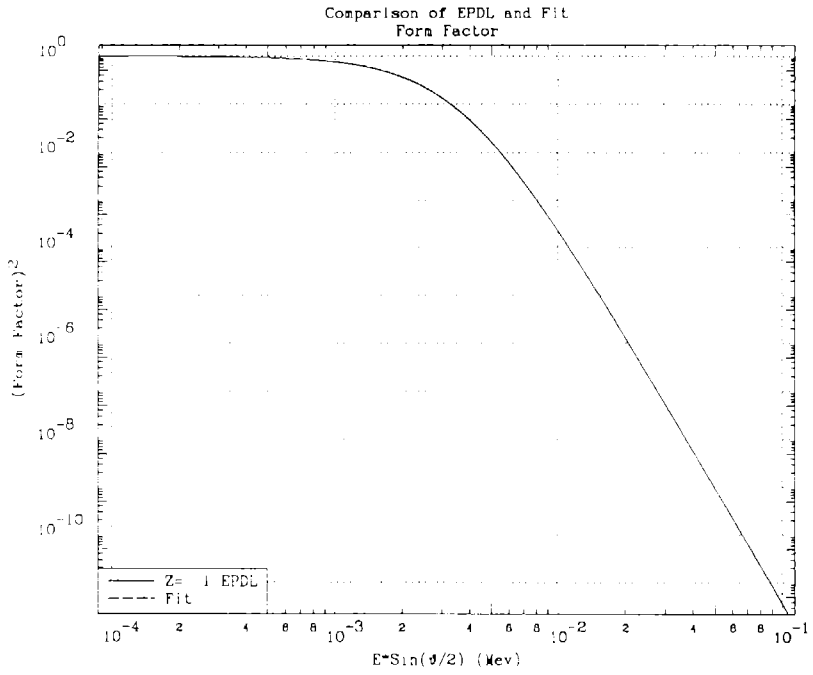
Comparison of EPDL and Fit
Form Factor
(Form Factor)^2
E*Sin(ϑ/2) (Mev)
Z= 1 EPDL
Fit

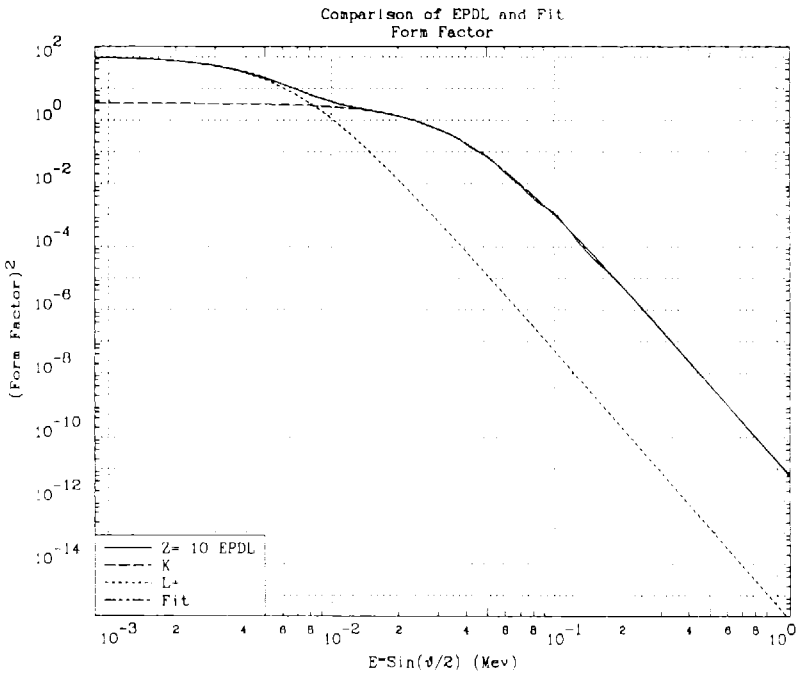
Comparison of EPDL and Fit
Form Factor
(Form Factor)^2
E*Sin(ϑ/2) (Mev)
Z= 10 EPDL
K
L+
Fit

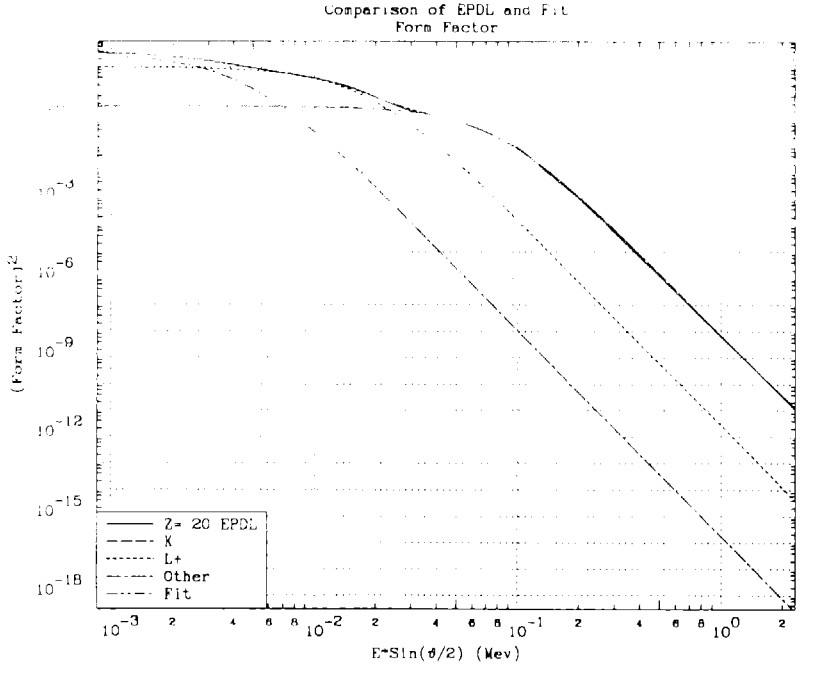
Comparison of EPDL and Fit
Form Factor
(Form Factor)^2
E*Sin(ϑ/2) (Mev)
Z= 20 EPDL
K
L+
Other
Fit

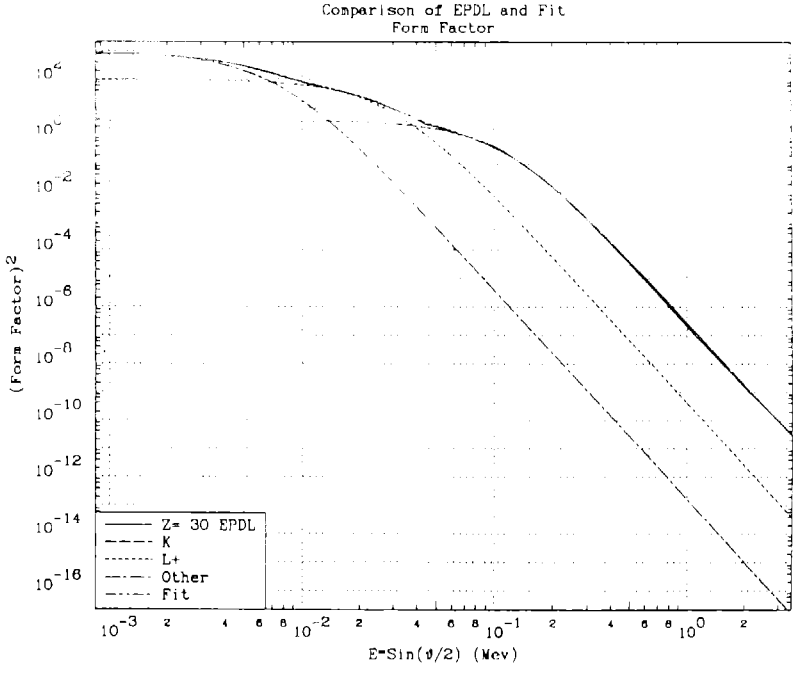
Comparison of EPDL and Fit
Form Factor
(Form Factor)^2
E*Sin(ϑ/2) (Mev)
Z= 30 EPDL
K
L+
Other
Fit

Fig. 1

Fig. 7

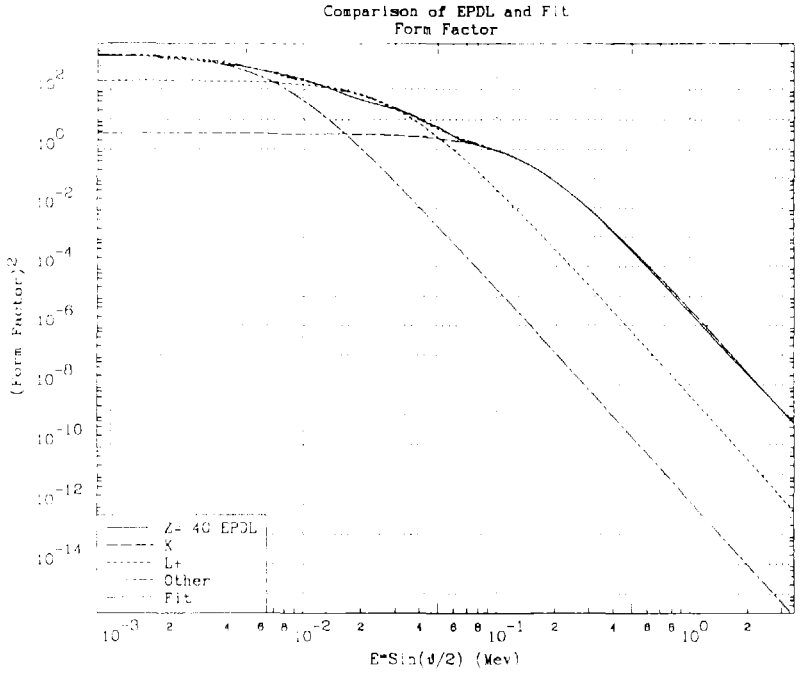
Comparison of EPDL and Fit
Form Factor
(Form Factor)²
E*Sin(ϑ/2) (Mev)
Z= 40 EPDL
K
L+
Other
Fit

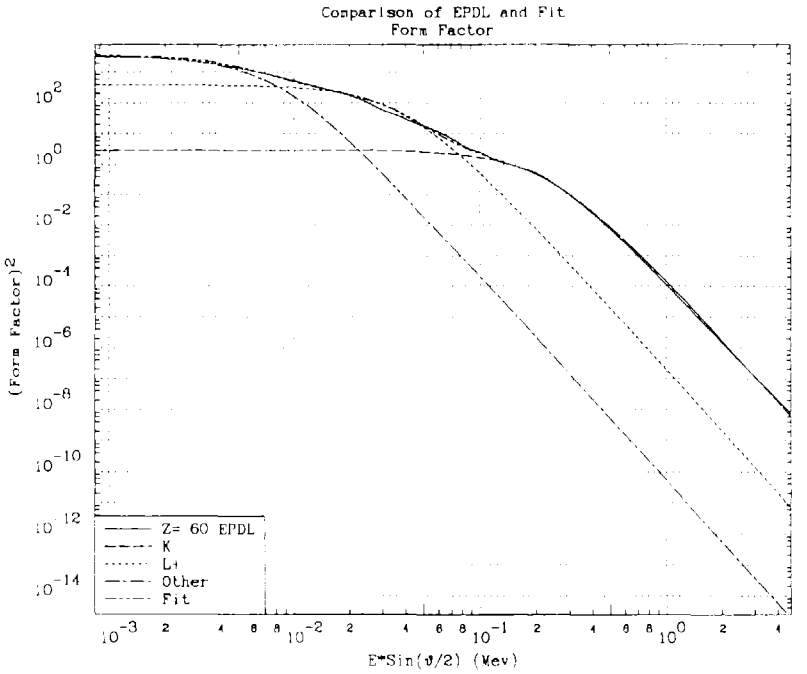
Comparison of EPDL and Fit
Form Factor
(Form Factor)²
E*Sin(ϑ/2) (Mev)
Z= 60 EPDL
K
L+
Other
Fit

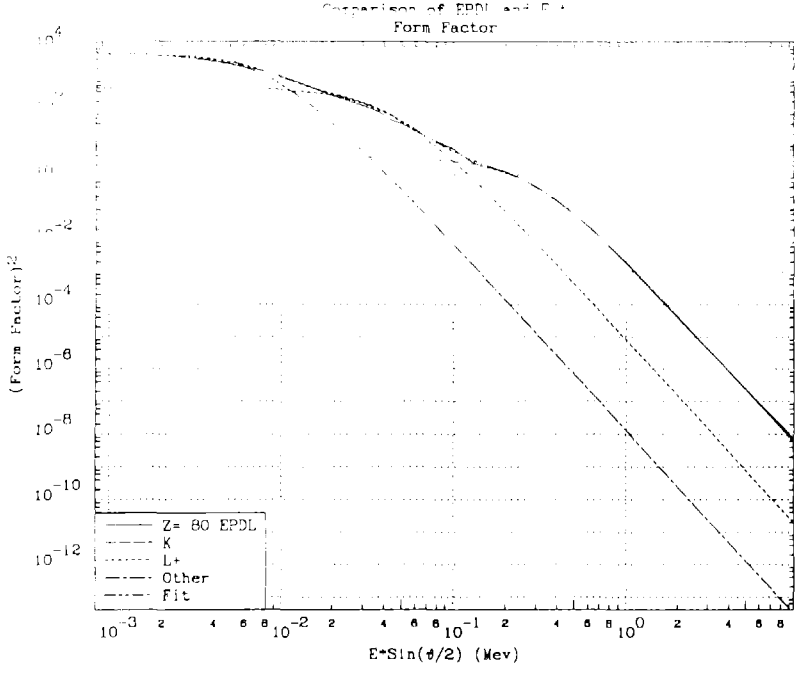
Form Factor
(Form Factor)²
E*Sin(ϑ/2) (Mev)
Z= 80 EPDL
K
L+
Other
Fit

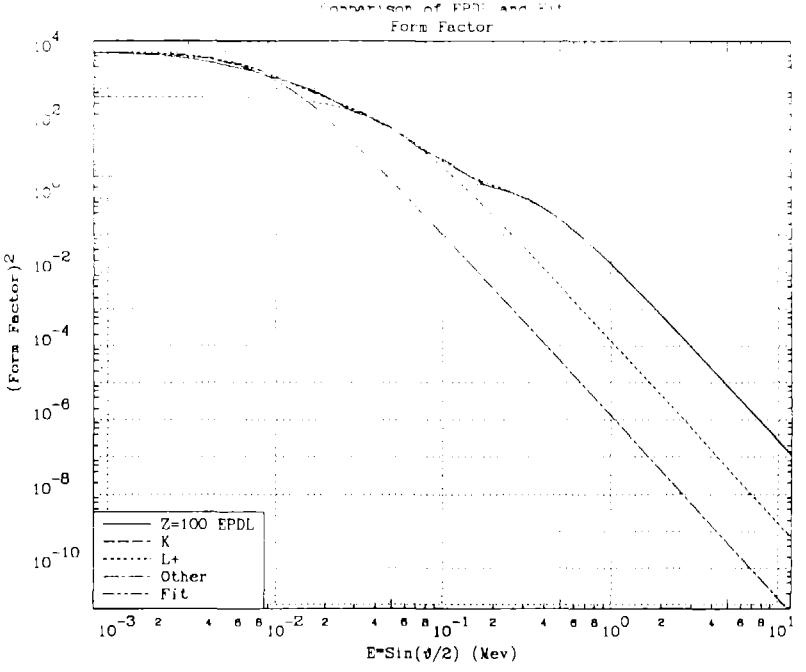
Form Factor
(Form Factor)²
E*Sin(ϑ/2) (Mev)
Z=100 EPDL
K
L+
Other
Fit

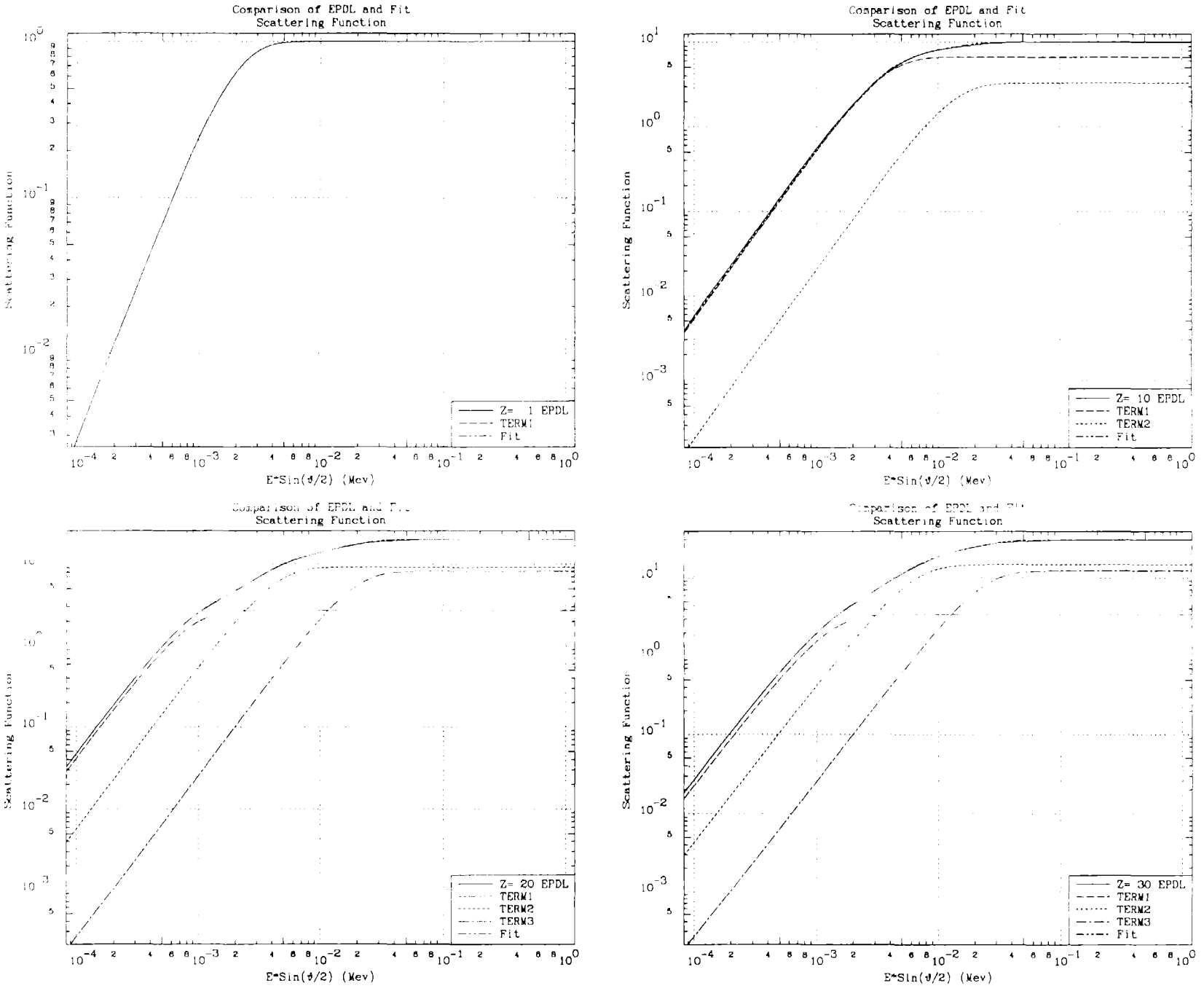
Comparison of EPDL and Fit
Scattering Function
Scattering Function
E*Sin(ϑ/2) (Mev)
Z= 1 EPDL
TERM1
Fit
Comparison of EPDL and Fit
Scattering Function
Scattering Function
E*Sin(ϑ/2) (Mev)
Z= 10 EPDL
TERM1
TERM2
Fit
Scattering Function
Scattering Function
E*Sin(ϑ/2) (Mev)
Z= 20 EPDL
TERM1
TERM2
TERM3
Fit
Scattering Function
Scattering Function
E*Sin(ϑ/2) (Mev)
Z= 30 EPDL
TERM1
TERM2
TERM3
Fit

FIG. 2

Fig. 4

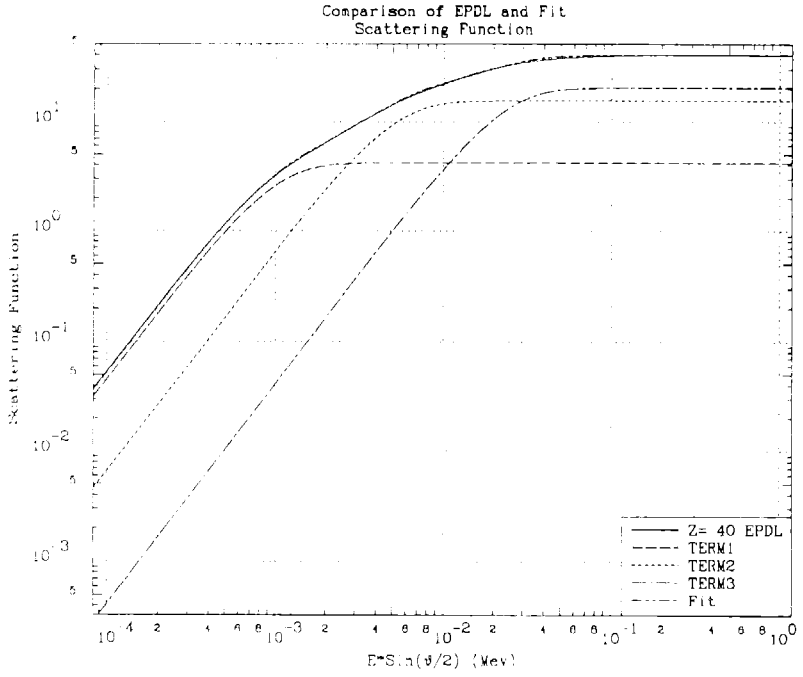
Comparison of EPDL and Fit
Scattering Function
Scattering Function
E=Sin(ϑ/2) (Mev)
Z= 40 EPDL
TERM1
TERM2
TERM3
Fit

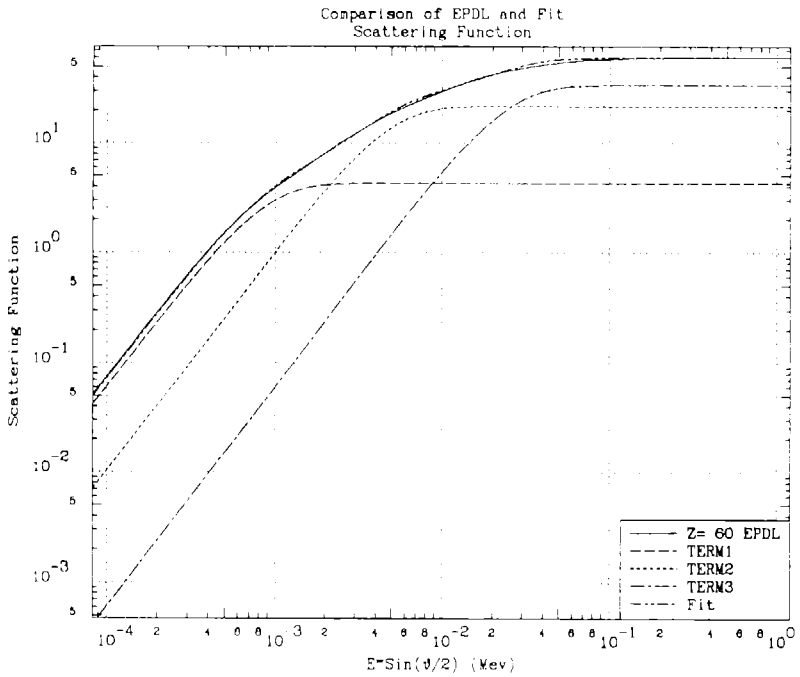
Comparison of EPDL and Fit
Scattering Function
Scattering Function
E=Sin(ϑ/2) (Mev)
Z= 60 EPDL
TERM1
TERM2
TERM3
Fit

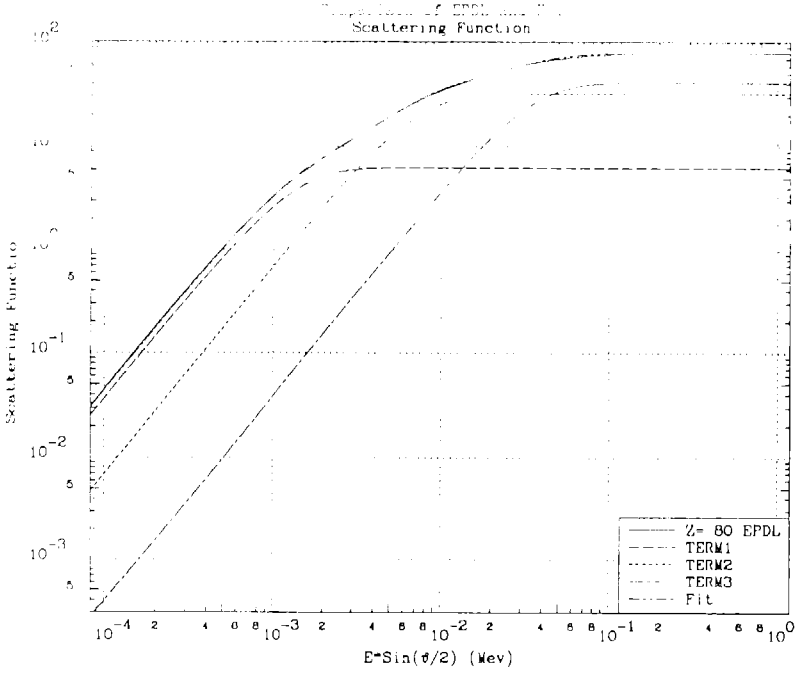
Scattering Function
Scattering Function
E=Sin(ϑ/2) (Mev)
Z= 80 EPDL
TERM1
TERM2
TERM3
Fit

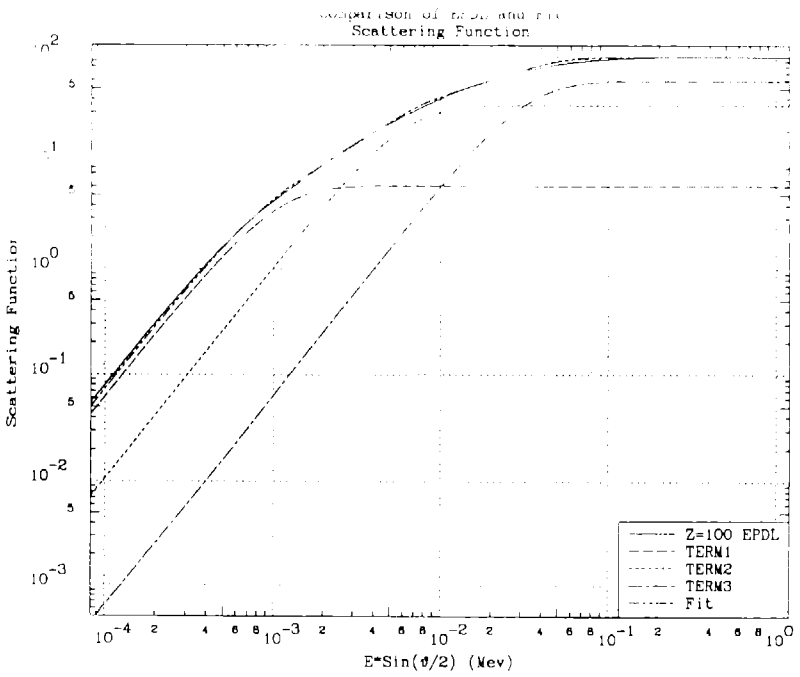
Scattering Function
Scattering Function
E=Sin(ϑ/2) (Mev)
Z=100 EPDL
TERM1
TERM2
TERM3
Fit

FIG. 1

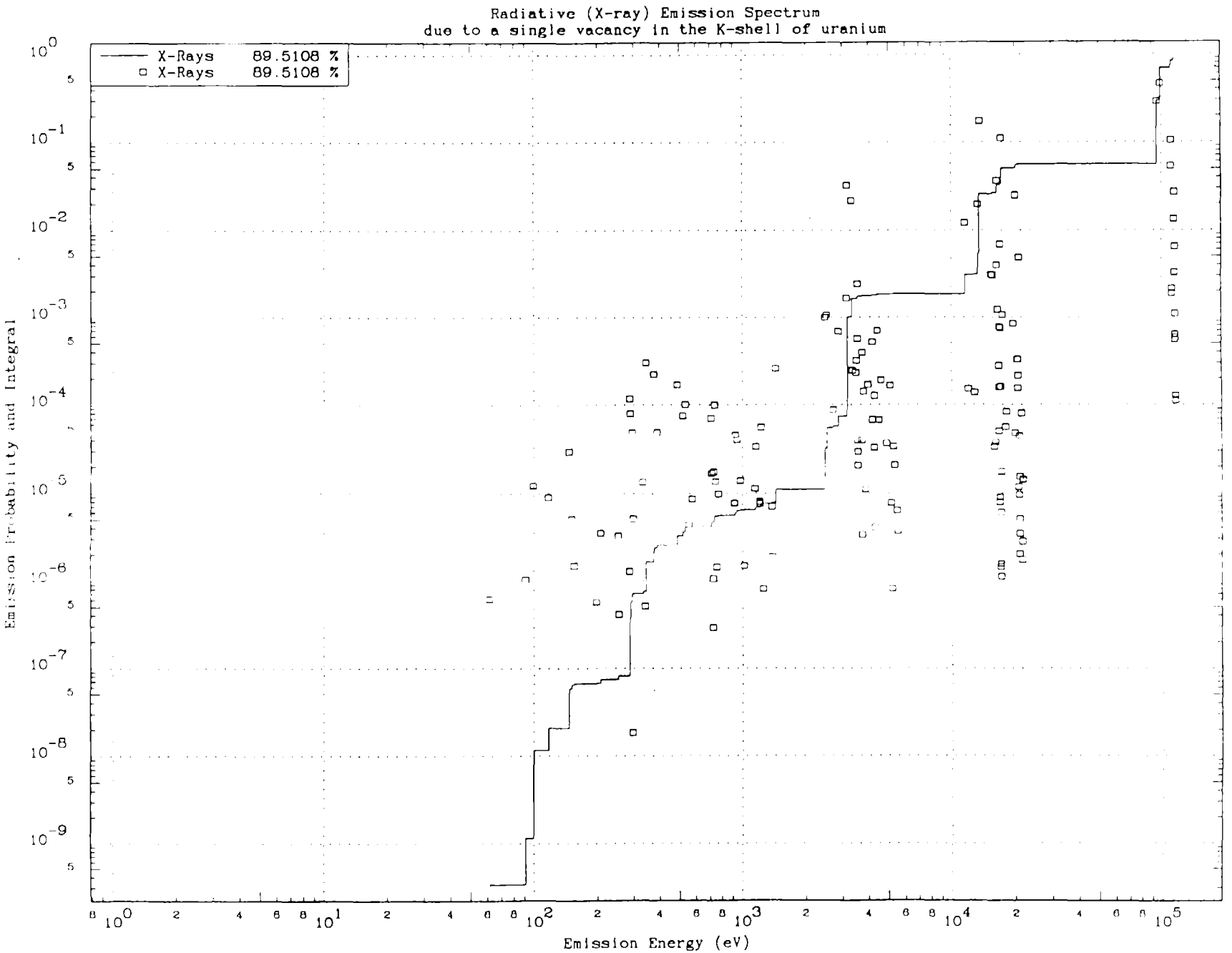
Radiative (X-ray) Emission Spectrum
due to a single vacancy in the K-shell of uranium
X-Rays 89.5108 %
X-Rays 89.5108 %
Emission Probability and Integral
Emission Energy (eV)

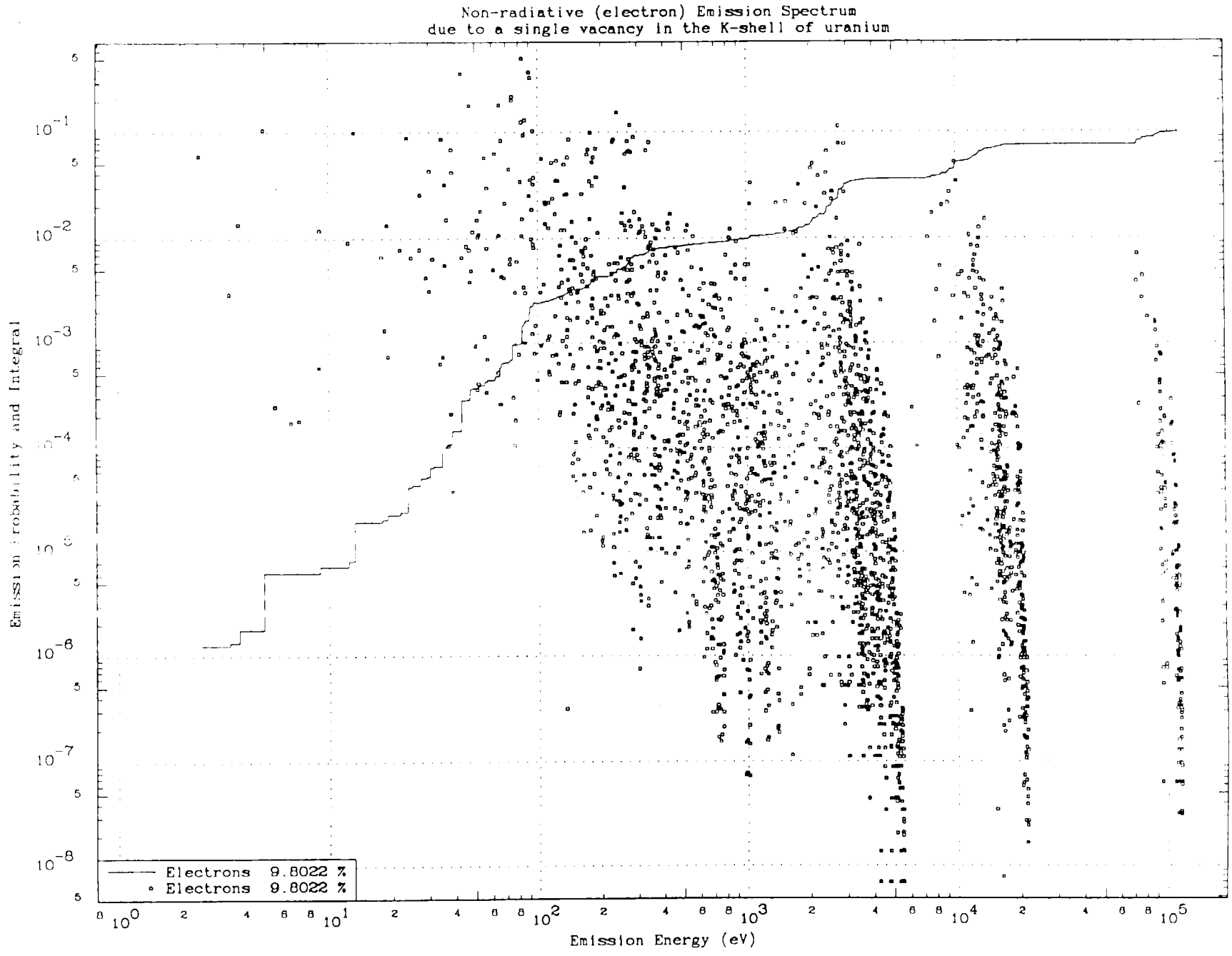
Non-radiative (electron) Emission Spectrum
due to a single vacancy in the K-shell of uranium
Emission Probability and Integral
Emission Energy (eV)
Electrons 9.8022 %
Electrons 9.8022 %

FIG. 5

EPICVIEW (Version 94-1)							Use MOUSE to Select Option
Lin/Log X	Zoom X	Grid + 1	Legend	Photons	Major	Z + 1	2 X 2
Lin/Log Y	Show All	Grid - 1	Bigger	Electrons	Minor	Z + 10	Listing
Points	Ratio		Smaller	Positrons	Deposit	Z - 1	Pstscript
	No Bottom			Charged	Range	Z - 10	
Freeze!!!	BottomsUp	barn-1/cm		Neutrons	Straggle	Same Z	Stop

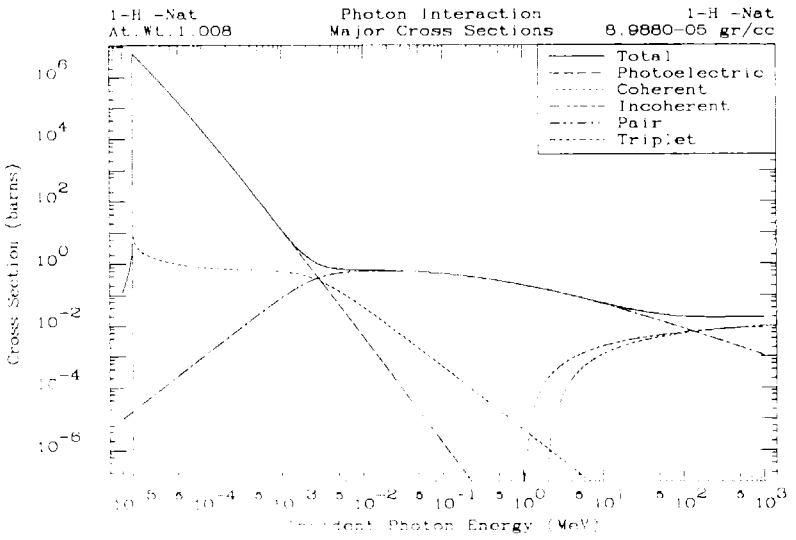

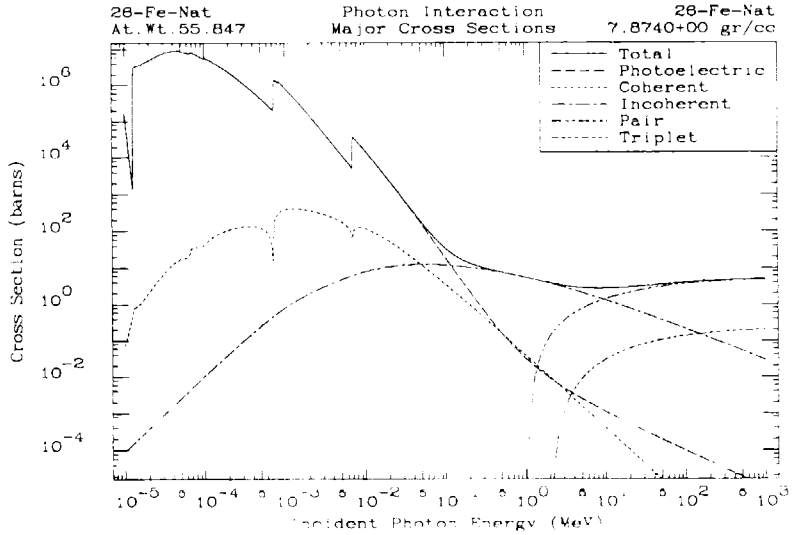

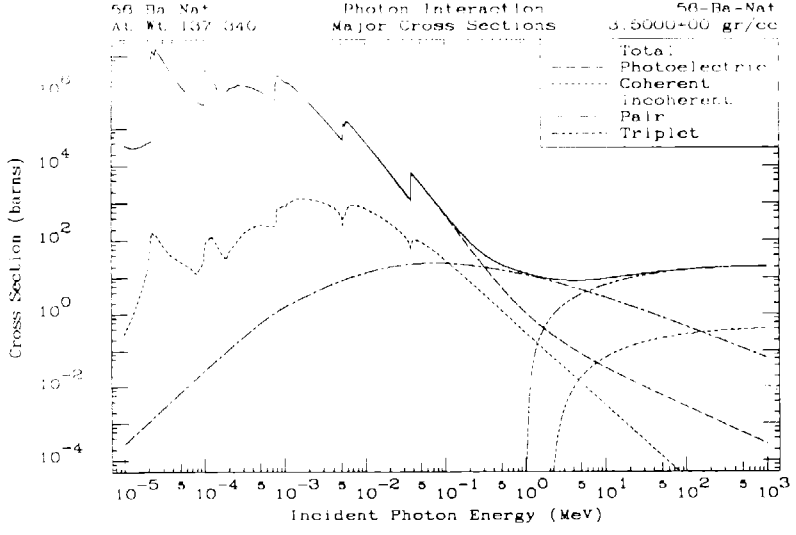

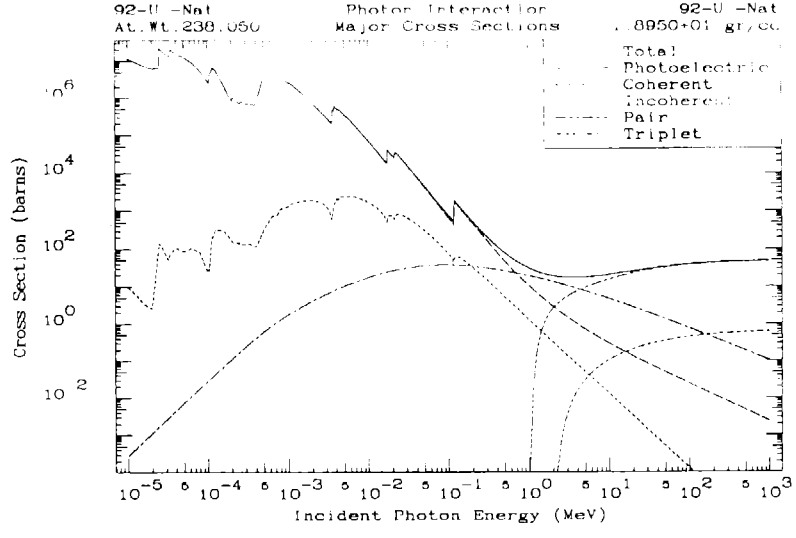

F16, 7

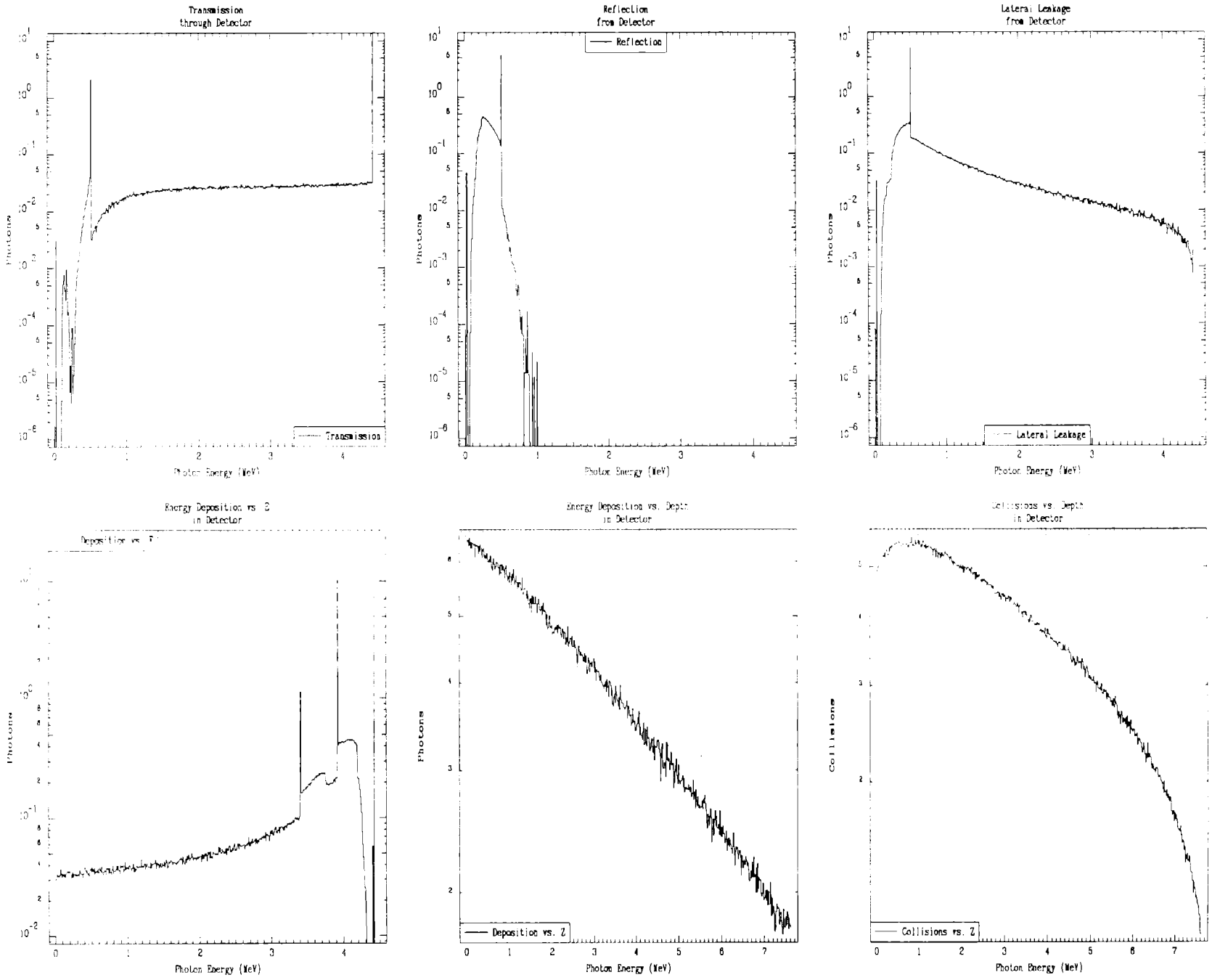
Transmission
through Detector
Photons
Photon Energy (MeV)
Transmission
Reflection
from Detector
Reflection
Lateral Leakage
from Detector
Lateral Leakage
Energy Deposition vs. Z
in Detector
Photons
Photon Energy (MeV)
Energy Deposition vs. Depth
in Detector
Deposition vs. Z
Collisions vs. Depth
in Detector
Collisions
Collisions vs. Z

FIG. 8

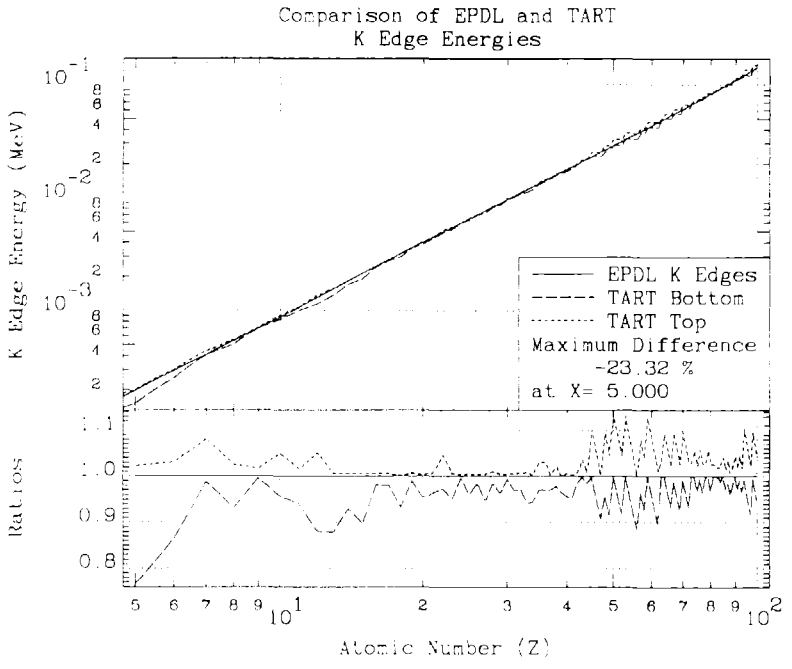
Comparison of EPDL and TART
K Edge Energies
K Edge Energy (MeV)
EPDL K Edges
TART Bottom
TART Top
Maximum Difference
-23.32 %
at X= 5.000
Ratios
Atomic Number (Z)

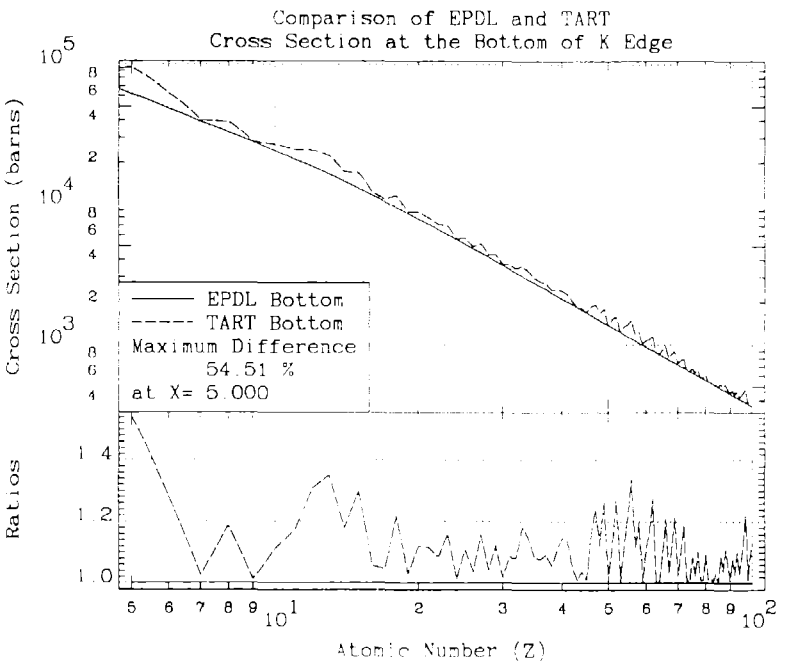
Comparison of EPDL and TART
Cross Section at the Bottom of K Edge
Cross Section (barns)
EPDL Bottom
TART Bottom
Maximum Difference
54.51 %
at X= 5.000
Ratios
Atomic Number (Z)

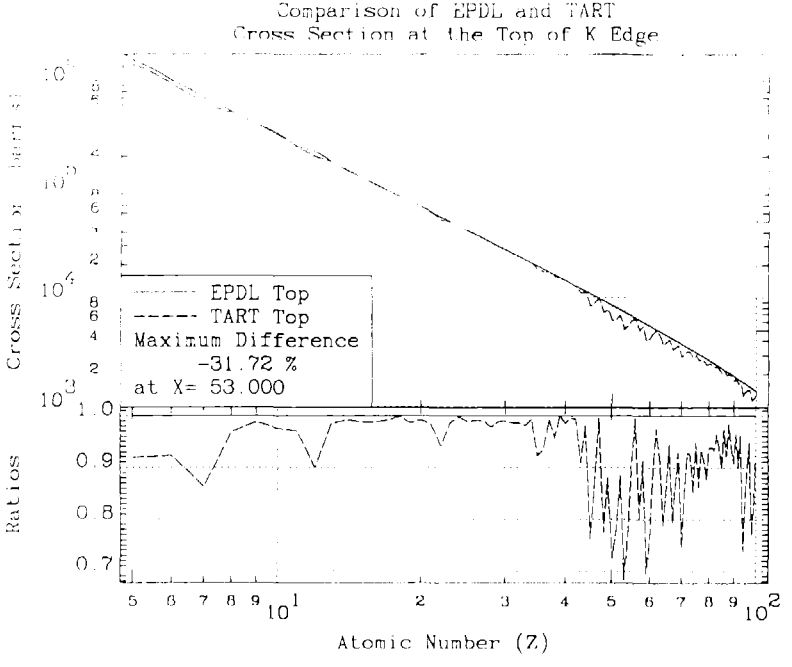
Comparison of EPDL and TART
Cross Section at the Top of K Edge
EPDL Top
TART Top
Maximum Difference
-31.72 %
at X= 53.000
Ratios
Atomic Number (Z)

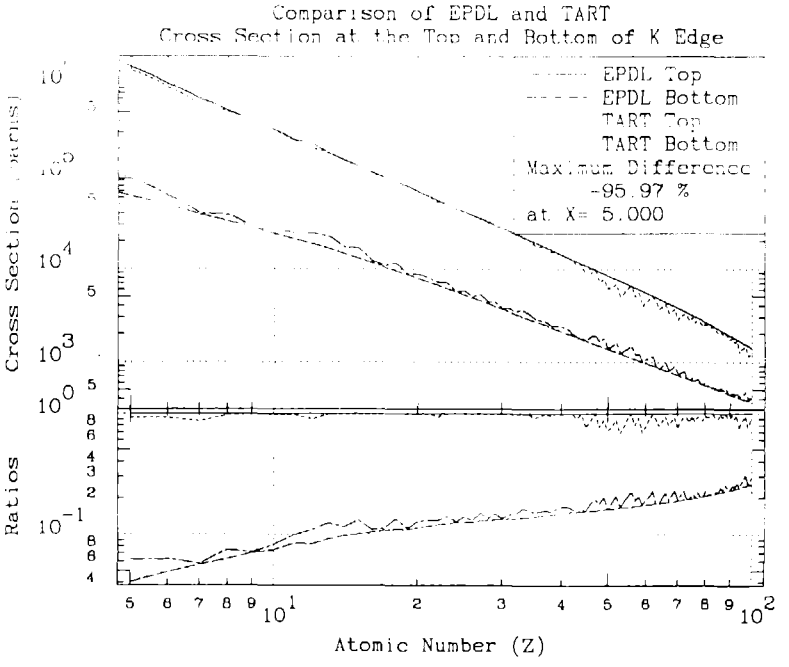
Comparison of EPDL and TART
Cross Section at the Top and Bottom of K Edge
EPDL Top
EPDL Bottom
TART Top
TART Bottom
Maximum Difference
-95.97 %
at X= 5.000
Ratios
Atomic Number (Z)

Fig. 9

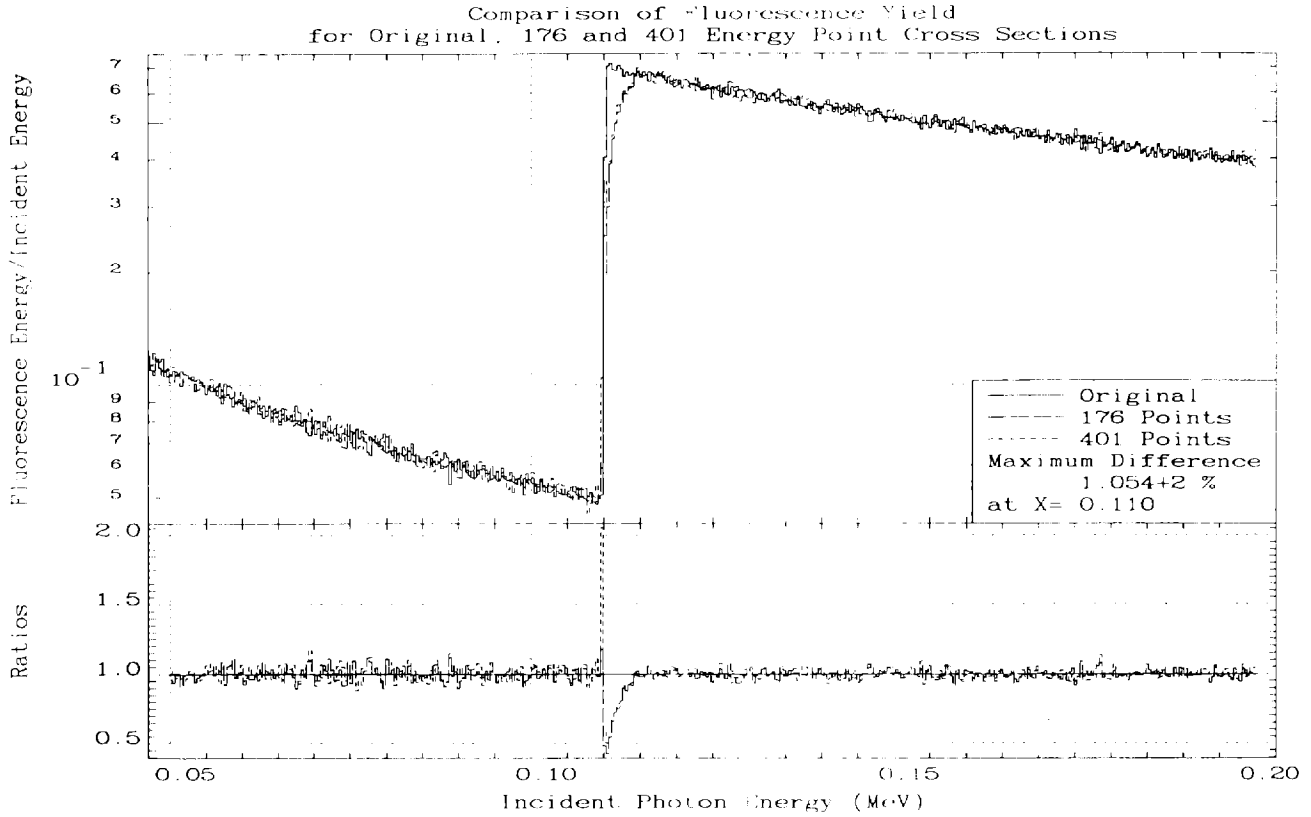
Comparison of Fluorescence Yield
for Original, 176 and 401 Energy Point Cross Sections
Fluorescence Energy/Incident Energy
Ratios
Original
176 Points
401 Points
Maximum Difference
1.054+2 %
at X= 0.110
0.05
0.10
0.15
0.20
Incident Photon Energy (MeV)

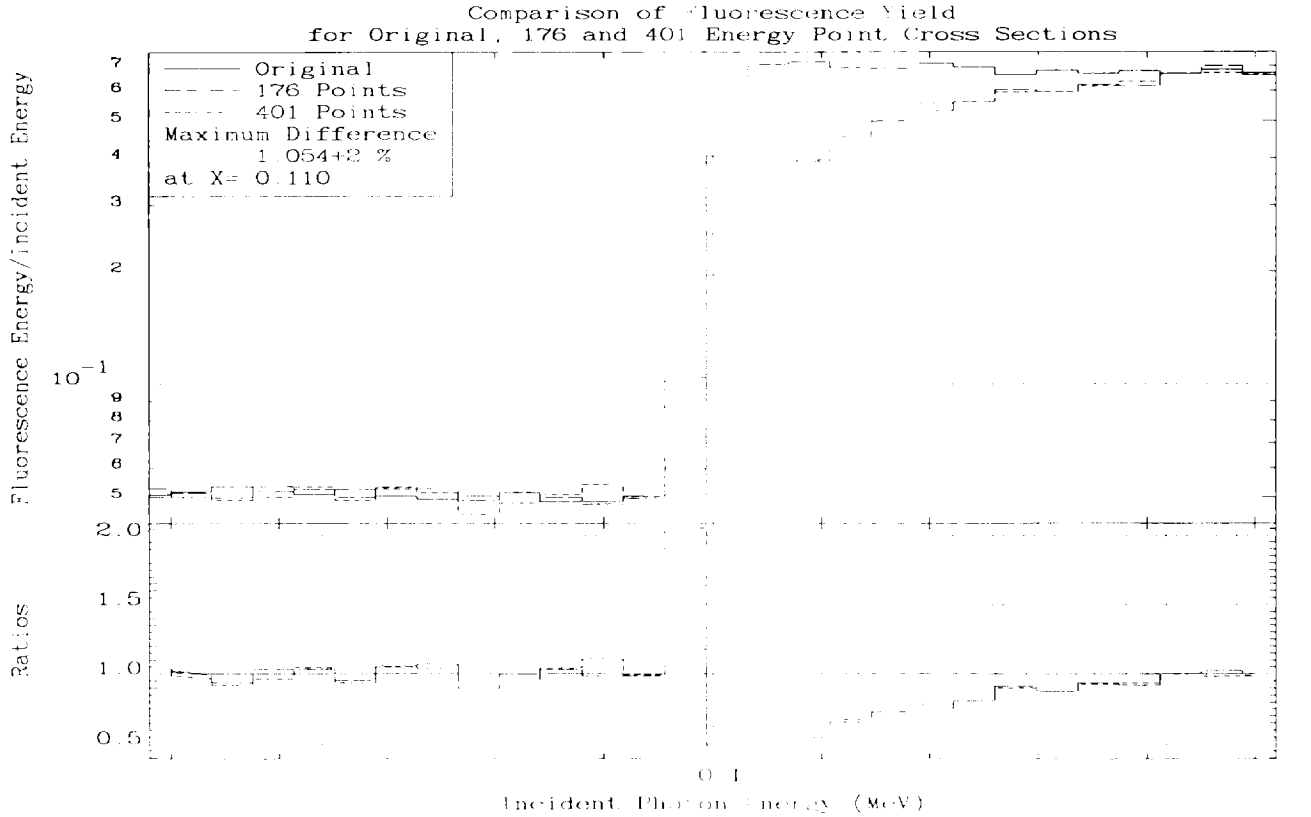
Comparison of Fluorescence Yield
for Original, 176 and 401 Energy Point Cross Sections
Fluorescence Energy/Incident Energy
Ratios
Original
176 Points
401 Points
Maximum Difference
1.054+2 %
at X= 0.110
Incident Photon Energy (MeV)

FIG. 10

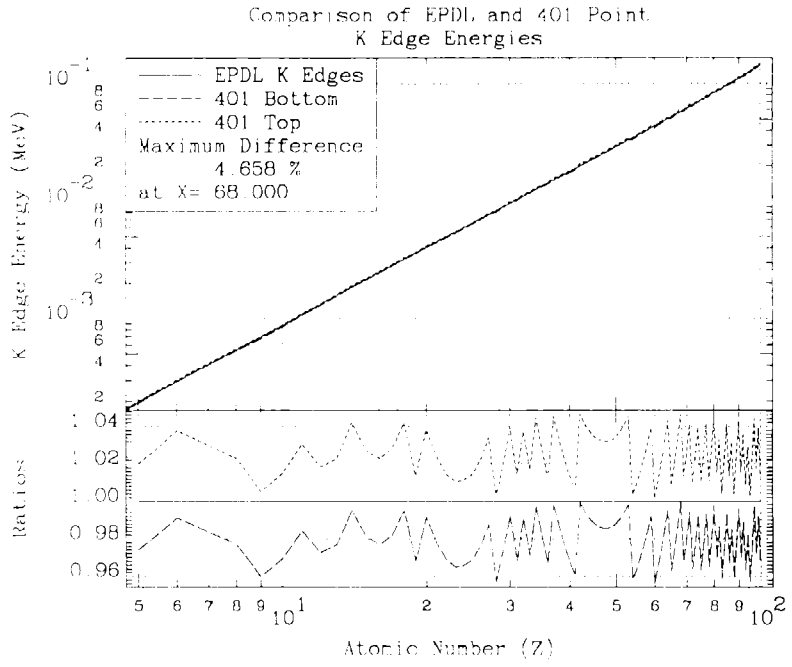
Comparison of EPDL and 401 Point
K Edge Energies
EPDL K Edges
401 Bottom
401 Top
Maximum Difference
4.658 %
at X= 68.000
K Edge Energy (MeV)
Ratios
Atomic Number (Z)

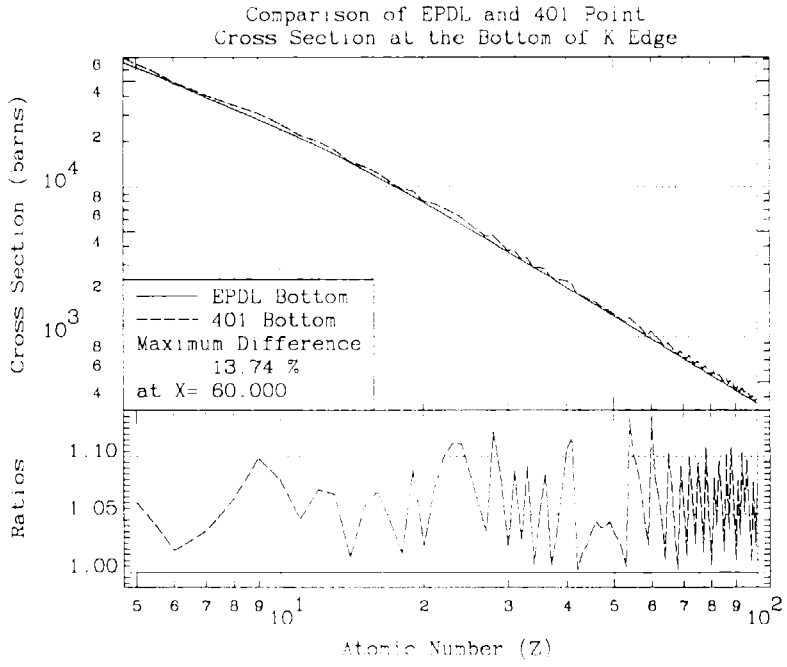
Comparison of EPDL and 401 Point
Cross Section at the Bottom of K Edge
EPDL Bottom
401 Bottom
Maximum Difference
13.74 %
at X= 60.000
Cross Section (barns)
Ratios
Atomic Number (Z)

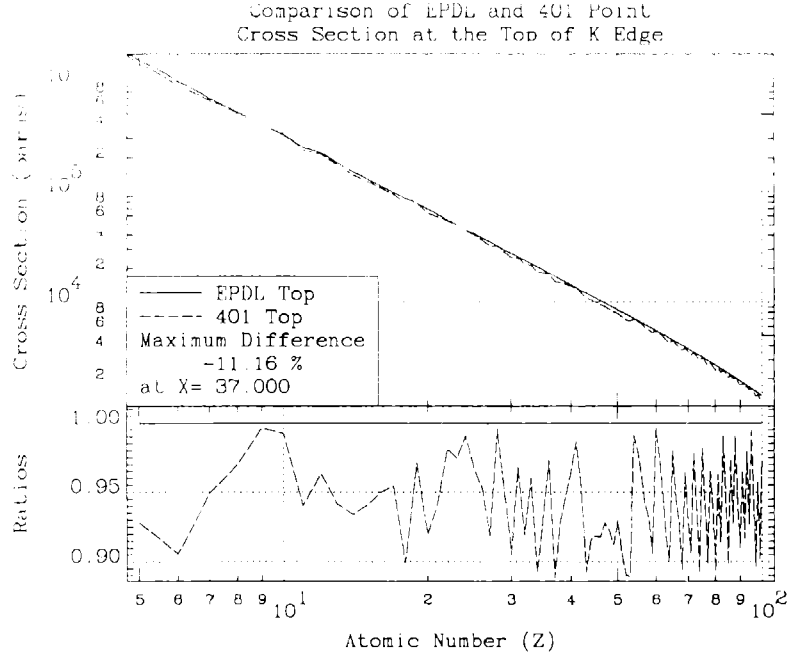
Comparison of EPDL and 401 Point
Cross Section at the Top of K Edge
EPDL Top
401 Top
Maximum Difference
-11.16 %
at X= 37.000
Cross Section (barns)
Ratios
Atomic Number (Z)

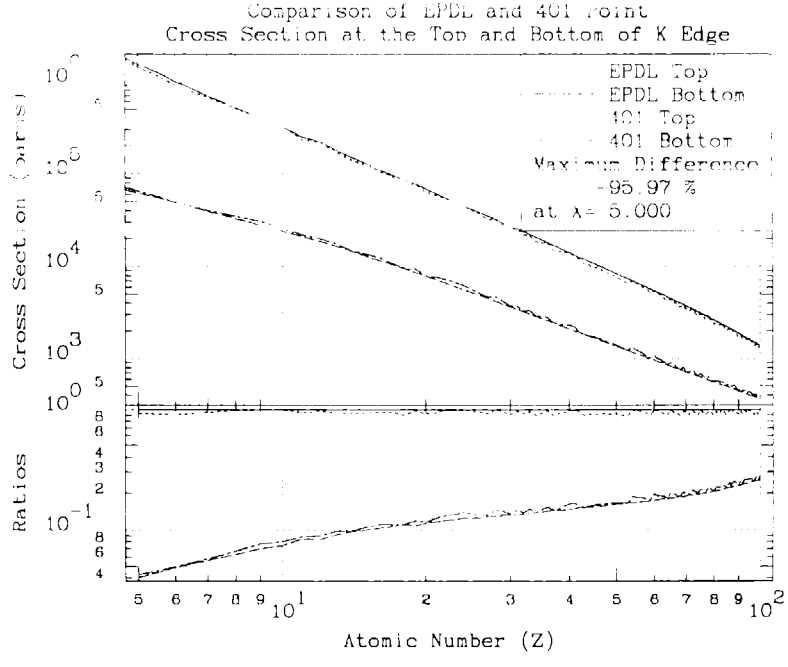
Comparison of EPDL and 401 Point
Cross Section at the Top and Bottom of K Edge
EPDL Top
EPDL Bottom
401 Top
401 Bottom
Maximum Difference
-95.97 %
at X= 5.000
Cross Section (barns)
Ratios
Atomic Number (Z)

Fig. 11

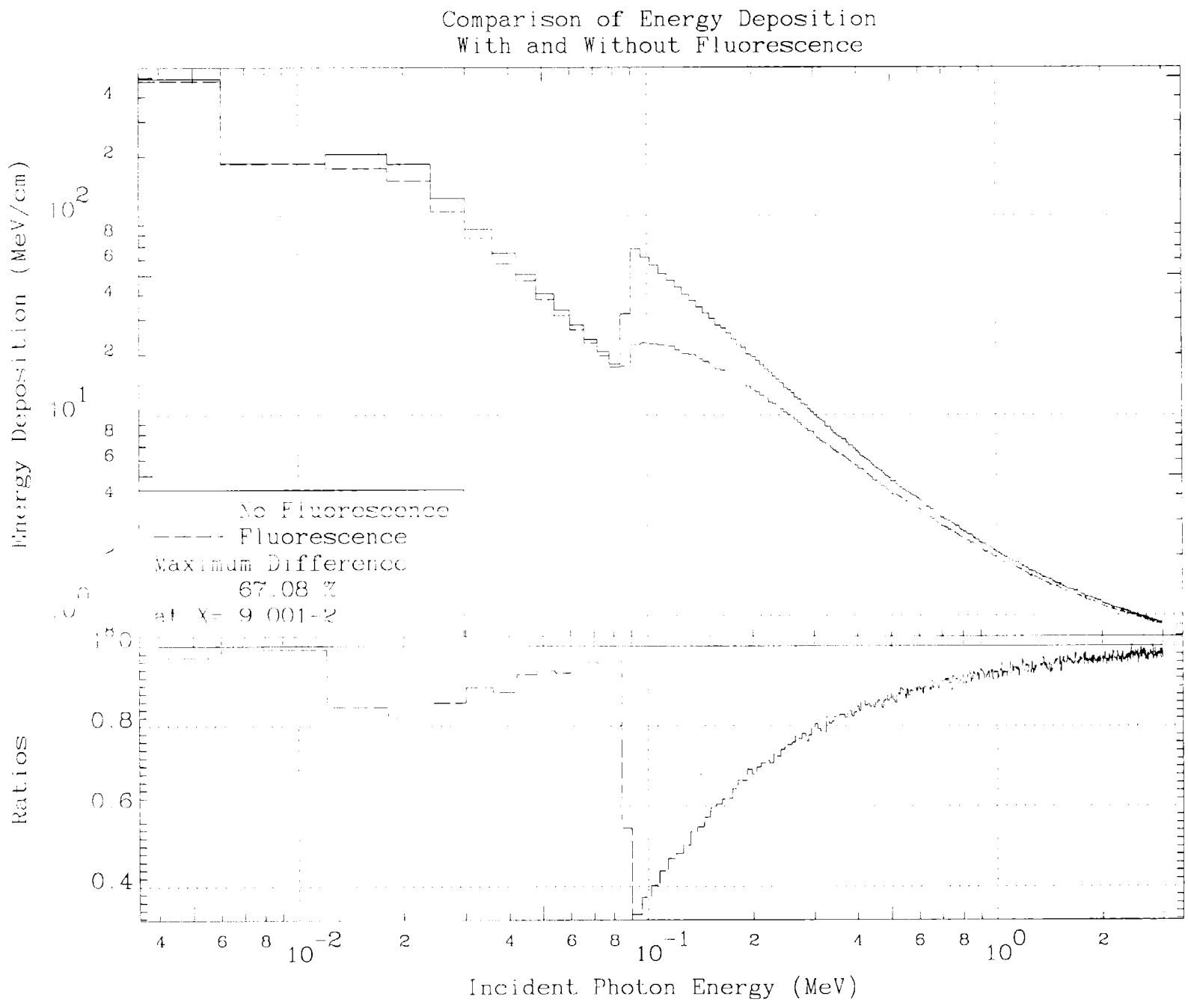
Comparison of Energy Deposition
With and Without Fluorescence
Energy Deposition (MeV/cm)
No Fluorescence
Fluorescence
Maximum Difference
67.08 %
Ratios
Incident Photon Energy (MeV)

Fig. 12

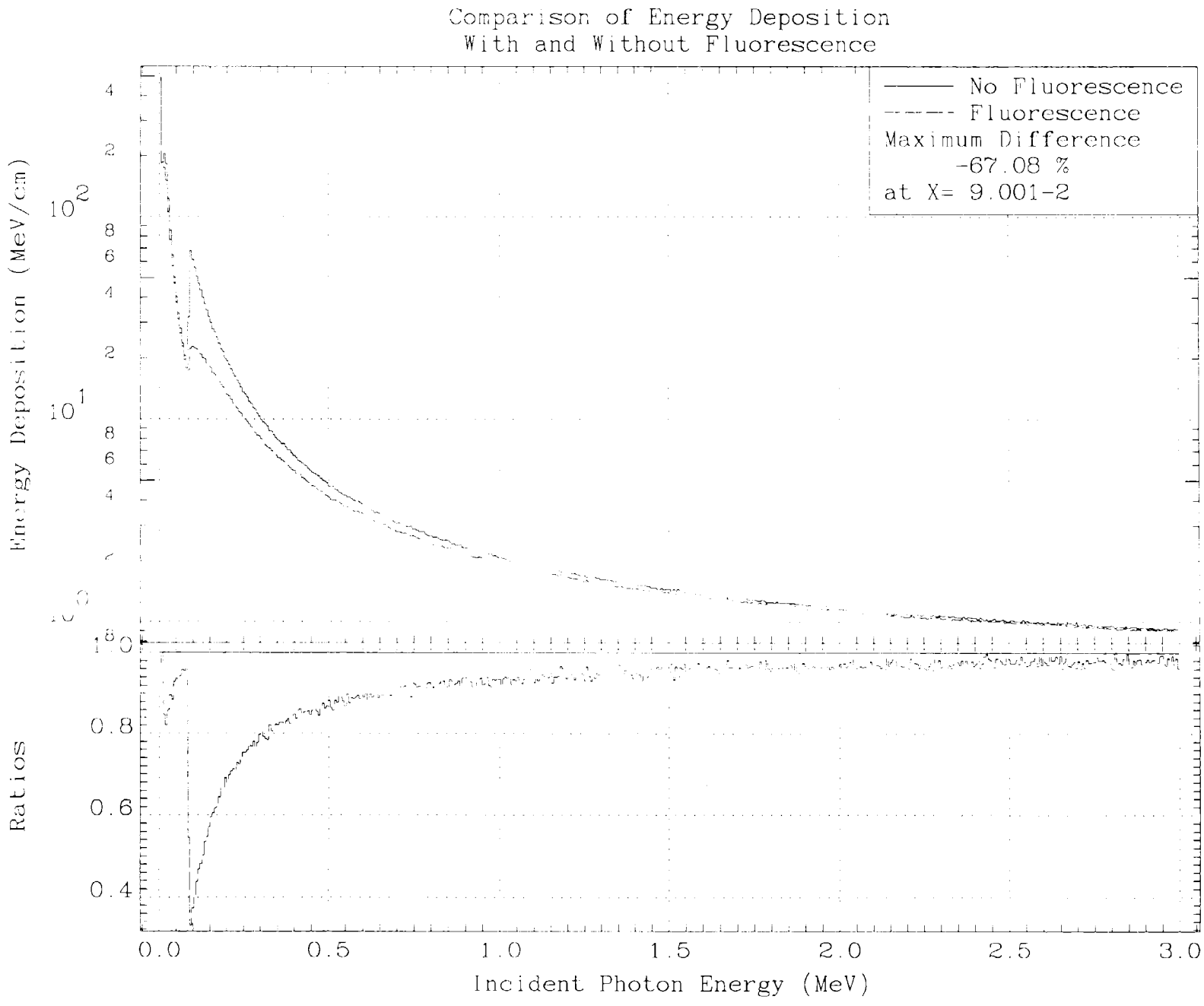
Comparison of Energy Deposition
With and Without Fluorescence
No Fluorescence
Fluorescence
Maximum Difference
-67.08 %
at X= 9.001-2
Energy Deposition (MeV/cm)
Ratios
Incident Photon Energy (MeV)
0.0
0.5
1.0
1.5
2.0
2.5
3.0
0.4
0.6
0.8

Fig. 15

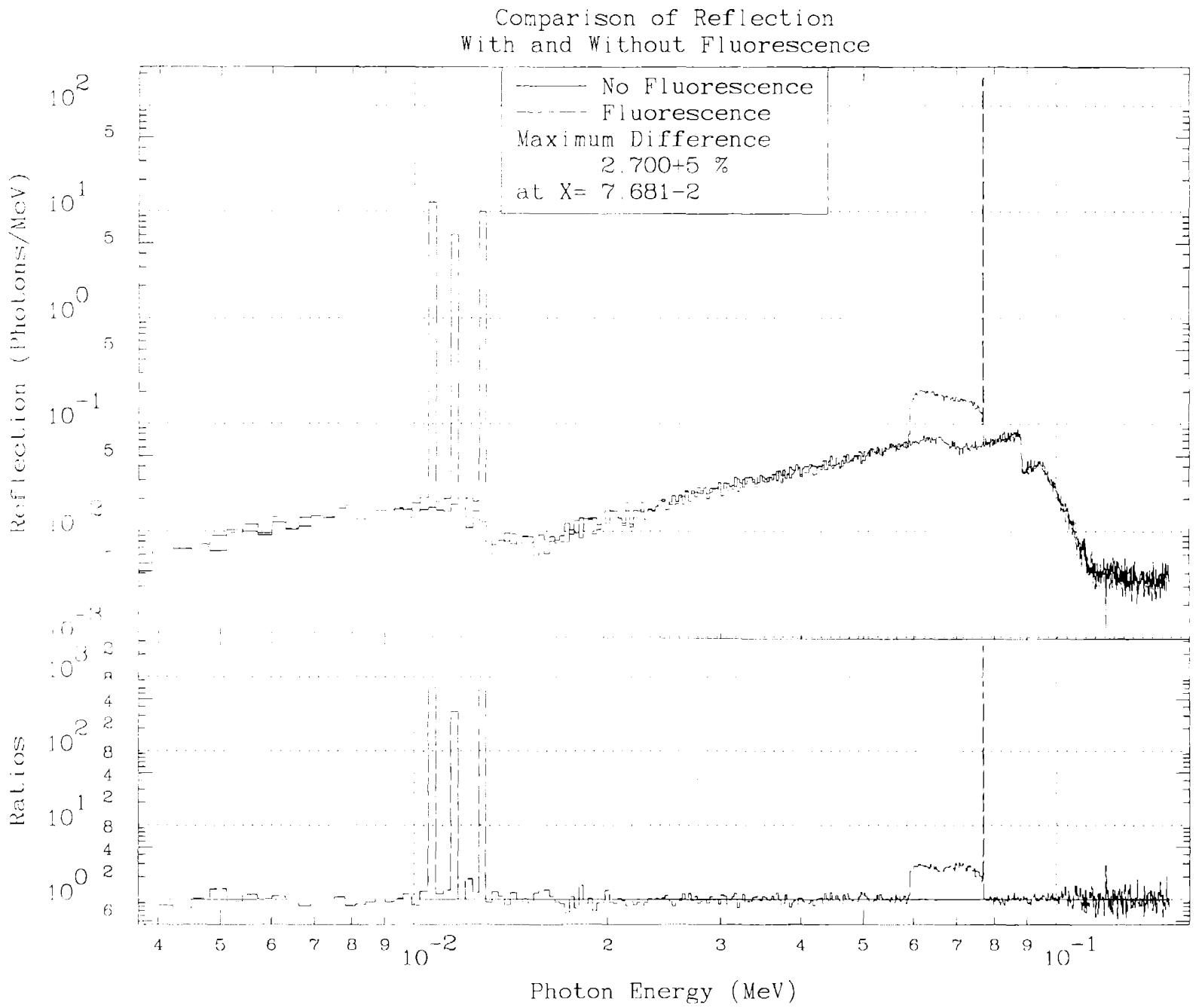
Comparison of Reflection
With and Without Fluorescence
No Fluorescence
Fluorescence
Maximum Difference
2.700+5 %
at X= 7.681-2
Reflection (Photons/MeV)
Ratios
Photon Energy (MeV)

Fig. 14

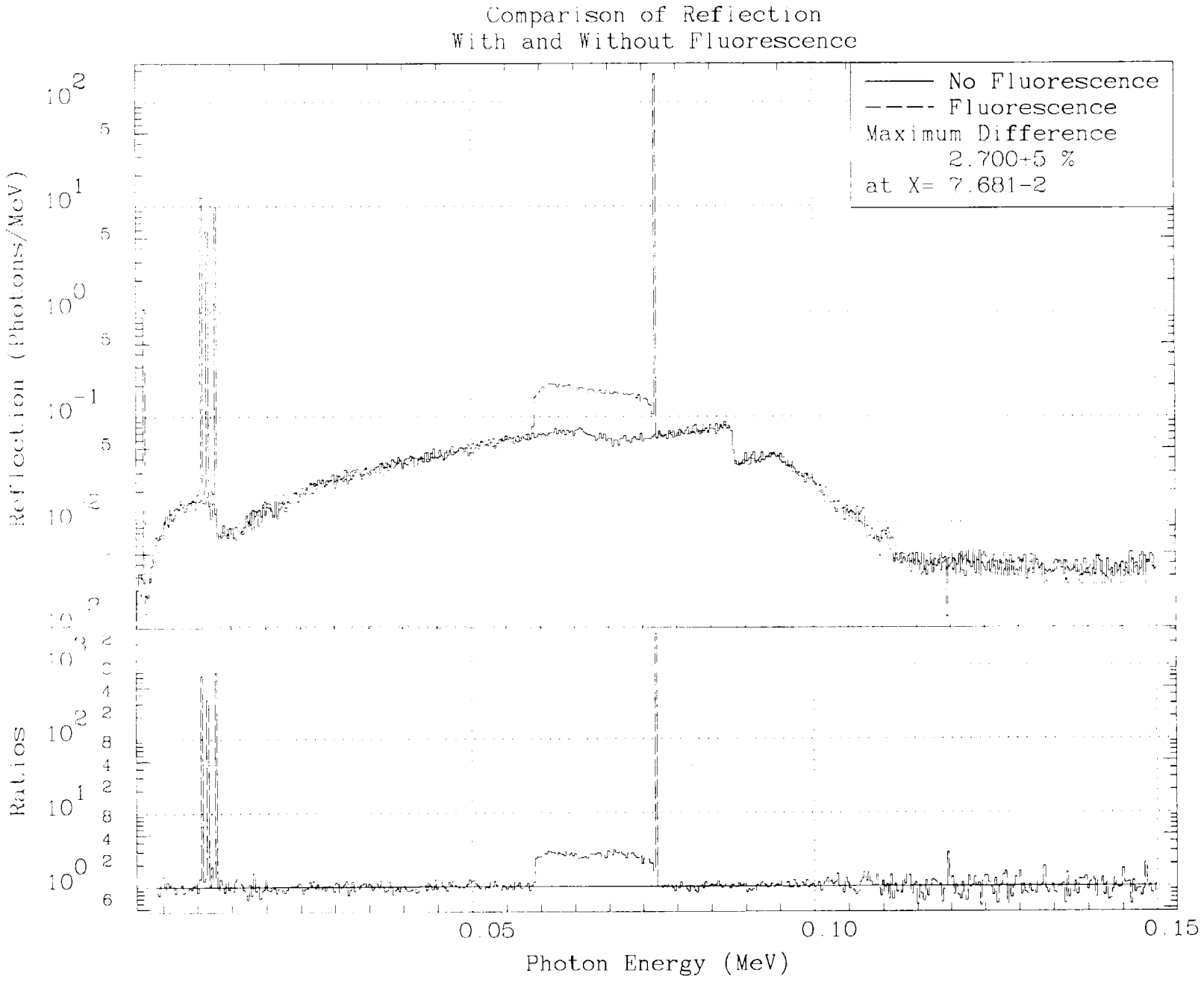
Comparison of Reflection
With and Without Fluorescence
No Fluorescence
Fluorescence
Maximum Difference
2.700+5 %
at X= 7.681-2
Reflection (Photons/MeV)
Ratios
0.05
0.10
0.15
Photon Energy (MeV)

Fig. 15

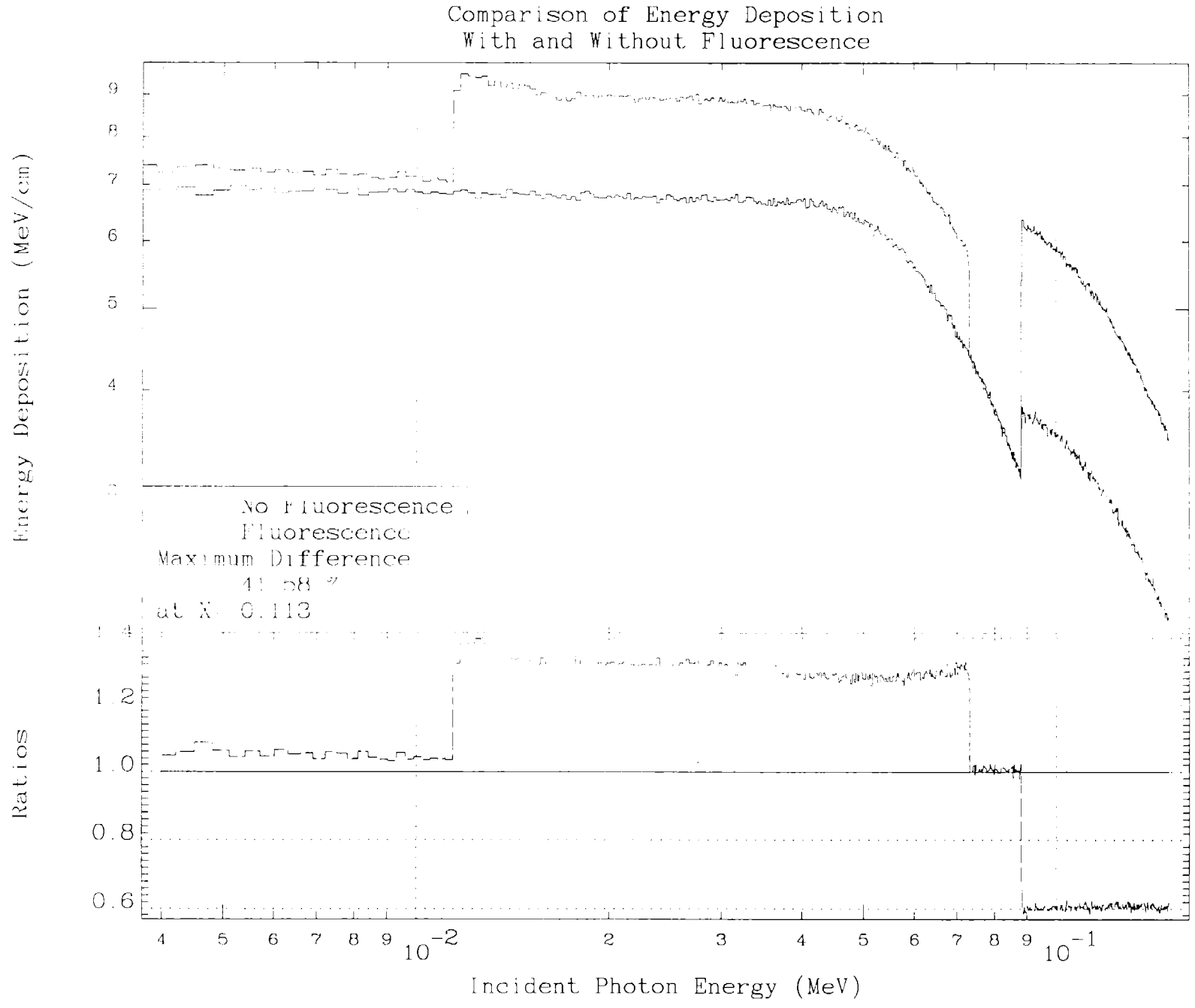
Comparison of Energy Deposition
With and Without Fluorescence
Energy Deposition (MeV/cm)
No Fluorescence
Fluorescence
Maximum Difference
41.58 %
at X= 0.113
Ratios
Incident Photon Energy (MeV)

Fig. 1c

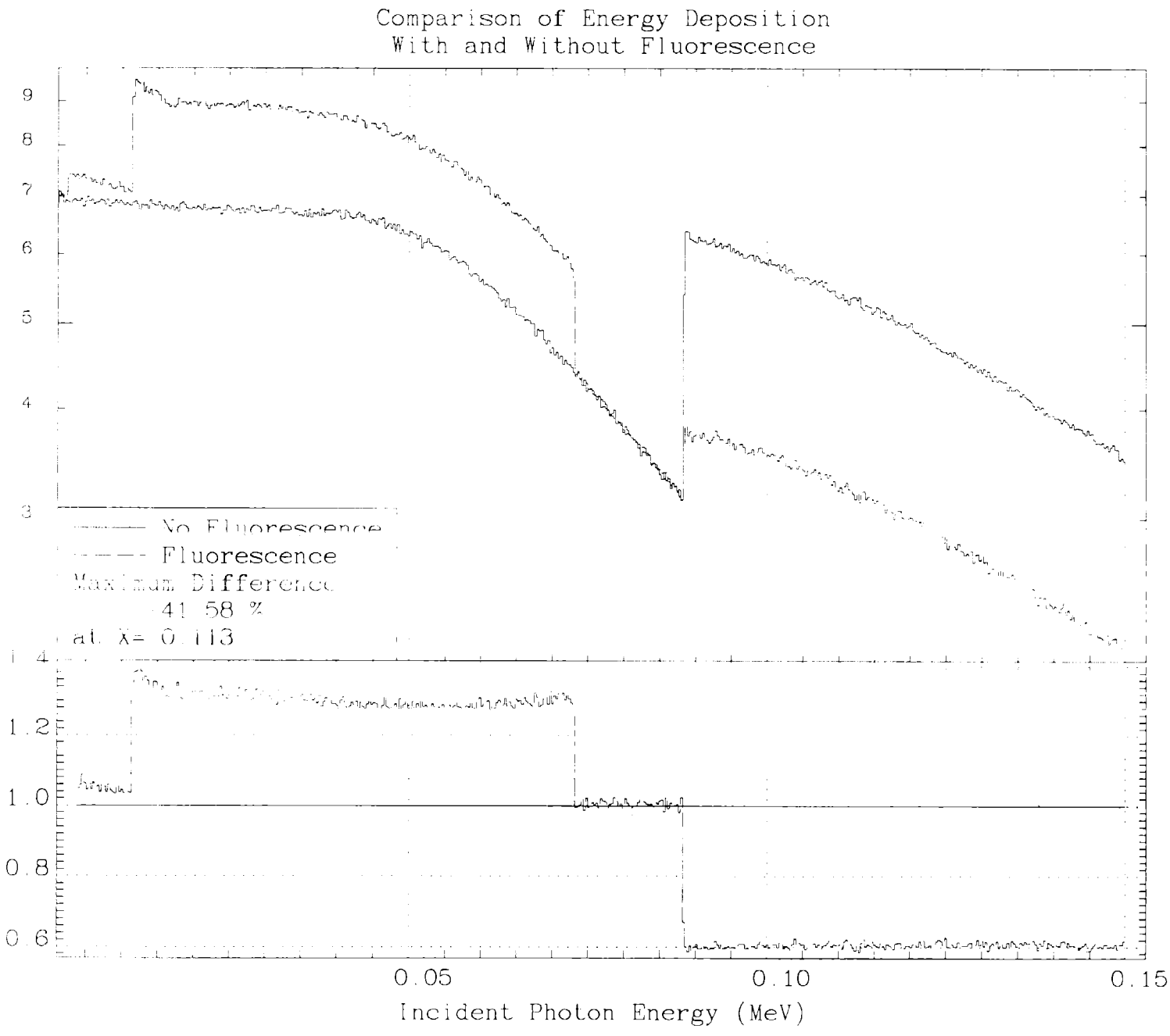
Comparison of Energy Deposition
With and Without Fluorescence
Energy Deposition (MeV/cm)
9
8
7
6
5
4
3
No Fluorescence
Fluorescence
Maximum Difference
41.58 %
at X= 0.113
Ratios
1.4
1.2
1.0
0.8
0.6
0.05
0.10
0.15
Incident Photon Energy (MeV)

Fig. 17

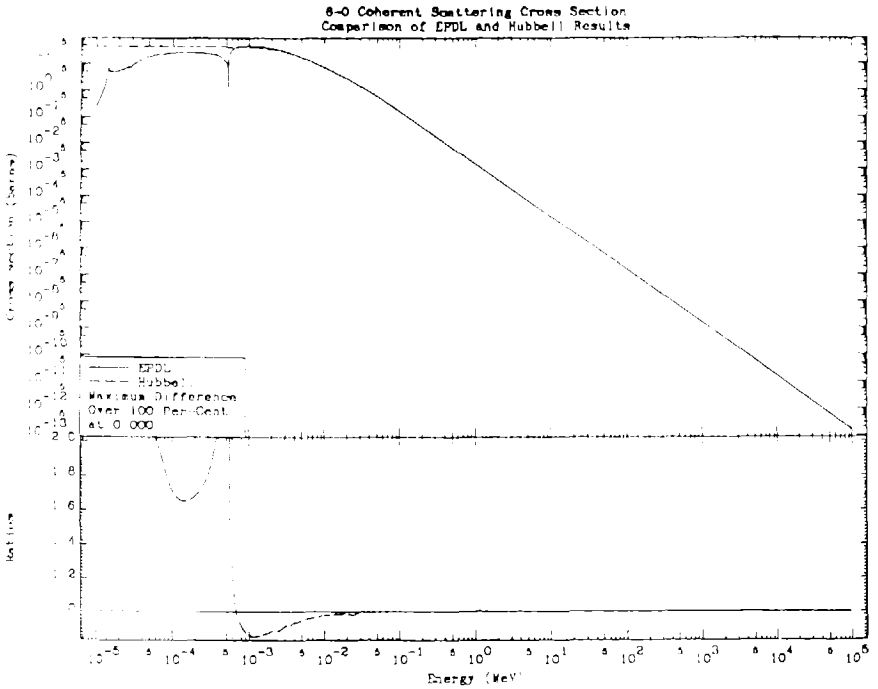
8-O Coherent Scattering Cross Section
Comparison of EPDL and Hubbell Results
EPDL
Hubbell
Maximum Difference
Over 100 Per-Cent
at 0.000
Ratios
Energy (MeV)

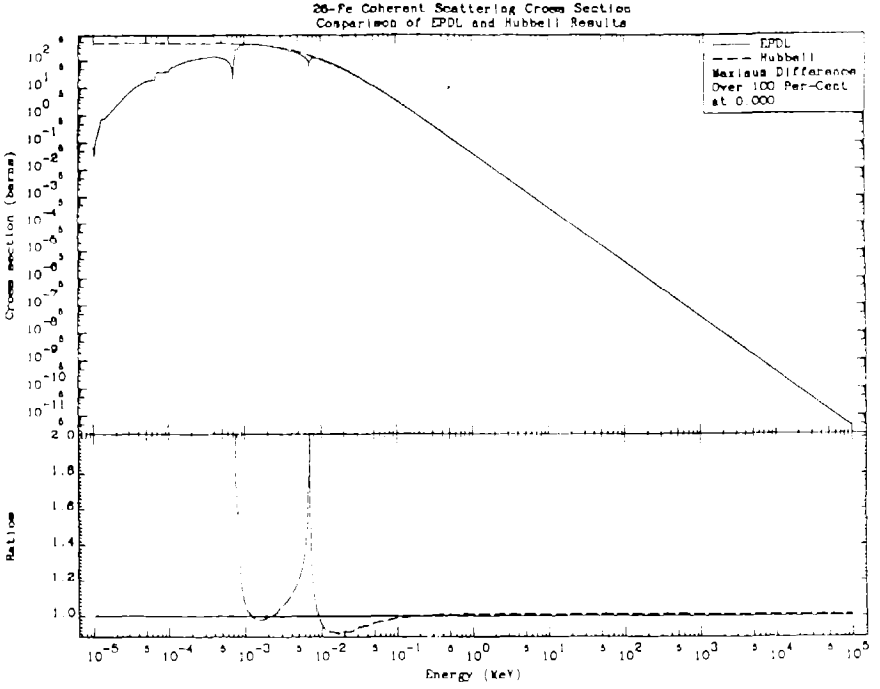
26-Fe Coherent Scattering Cross Section
Comparison of EPDL and Hubbell Results
EPDL
Hubbell
Maximum Difference
Over 100 Per-Cent
at 0.000
Cross section (barns)
Ratios
Energy (MeV)

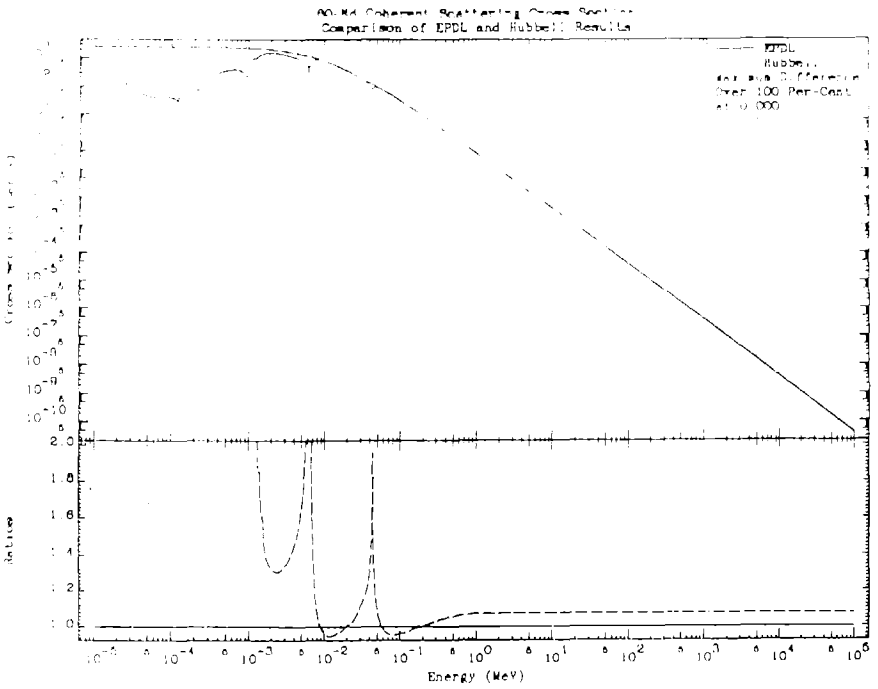
Comparison of EPDL and Hubbell Results
EPDL
Hubbell
Energy (MeV)

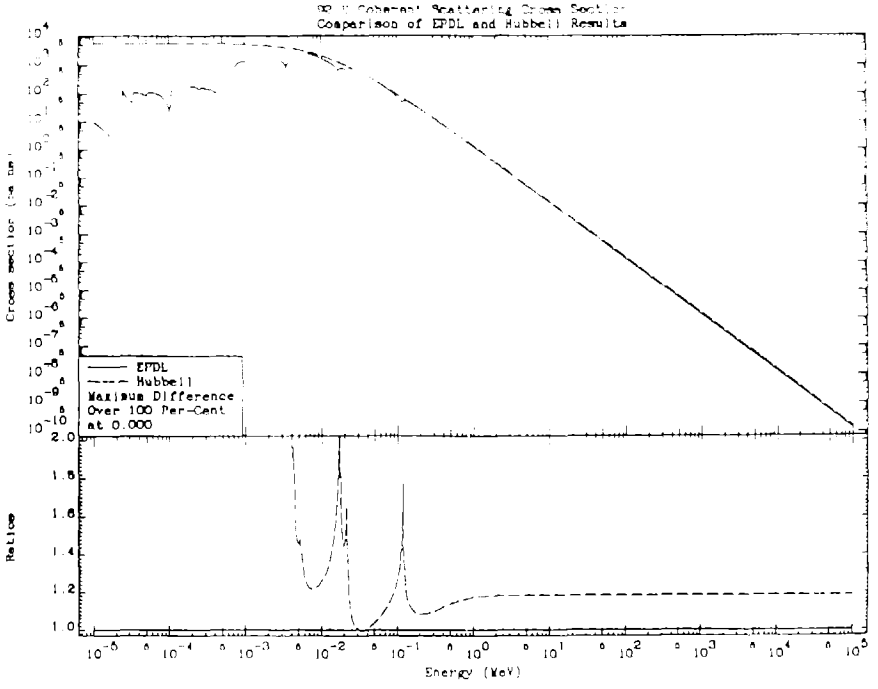
Comparison of EPDL and Hubbell Results
EPDL
Hubbell
Maximum Difference
Over 100 Per-Cent
at 0.000
Ratios
Energy (MeV)

Fig. 18

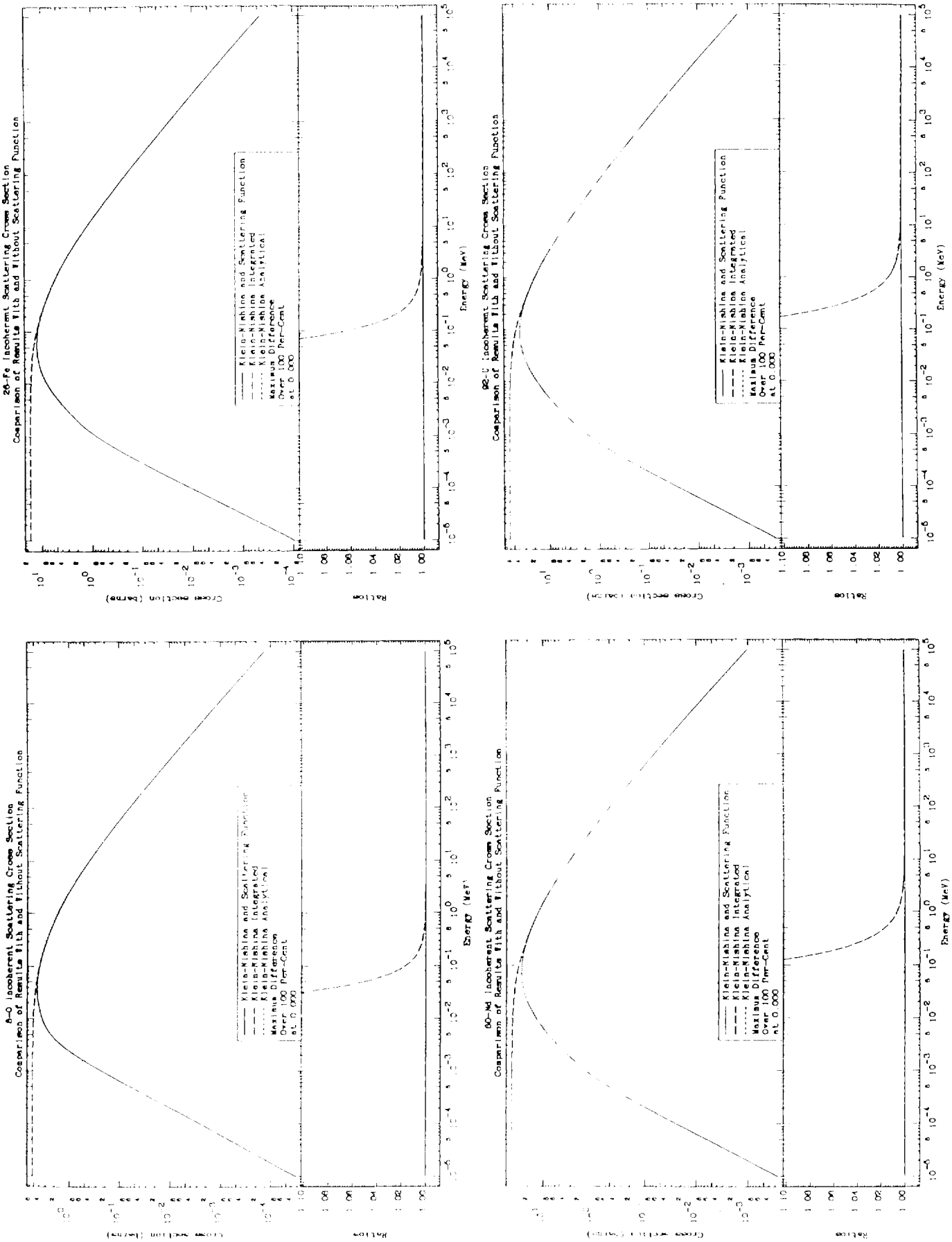
8-O Incoherent Scattering Cross Section
Comparison of Results With and Without Scattering Function
26-Fe Incoherent Scattering Cross Section
Comparison of Results With and Without Scattering Function
50-Nd Incoherent Scattering Cross Section
Comparison of Results With and Without Scattering Function
92-U Incoherent Scattering Cross Section
Comparison of Results With and Without Scattering Function
Klein-Nishina and Scattering Function
Klein-Nishina Integrated
Klein-Nishina Analytical
Maximum Difference
Over 100 Per-Cent
at 0.000
Energy (MeV)
Ratios
Cross section (barns)

FIG. 19

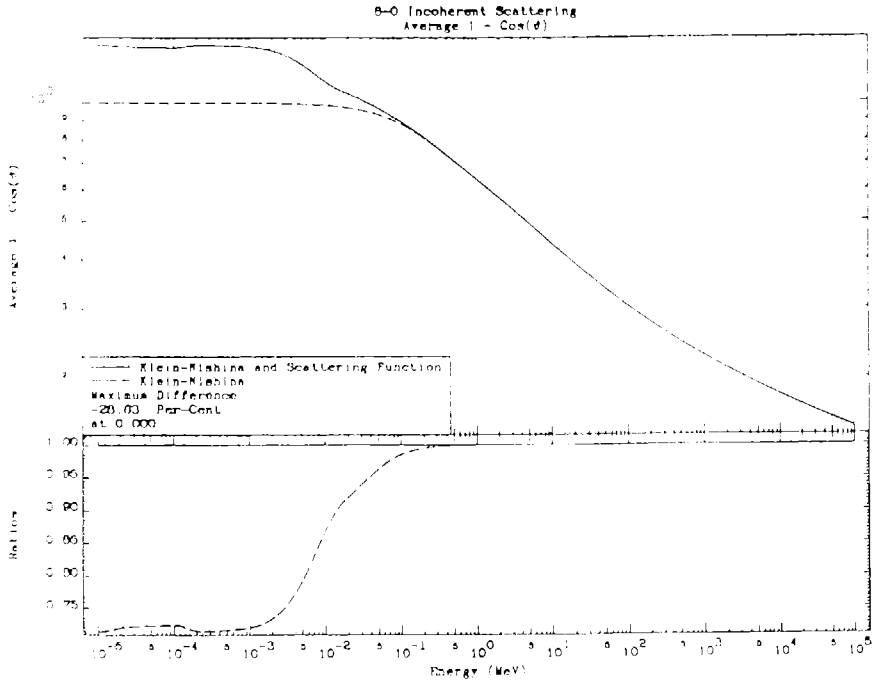
8-O Incoherent Scattering
Average 1 - Cos(θ)
Klein-Nishina and Scattering Function
Klein-Nishina
Maximum Difference
-20.03 Per-Cent
at 0.000
Ratio
Energy (MeV)

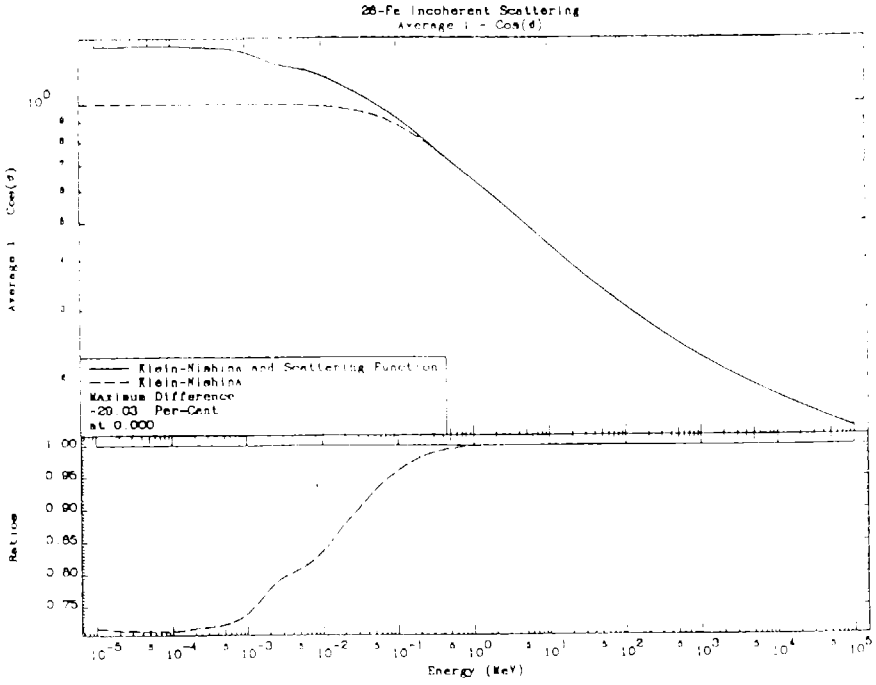
26-Fe Incoherent Scattering
Average 1 - Cos(θ)
Klein-Nishina and Scattering Function
Klein-Nishina
Maximum Difference
-20.03 Per-Cent
at 0.000
Ratio
Energy (MeV)

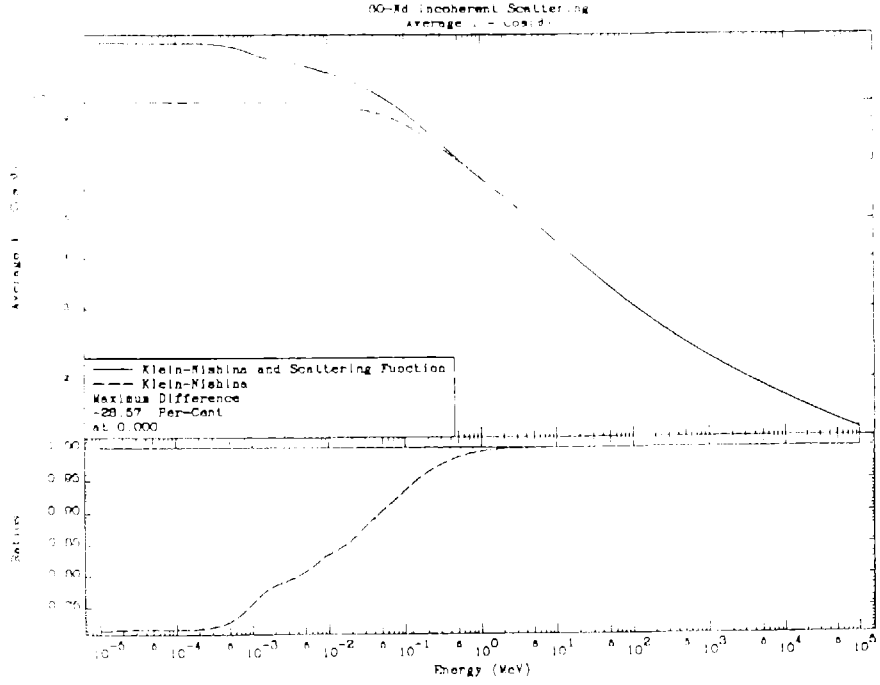
Klein-Nishina and Scattering Function
Klein-Nishina
Maximum Difference
-20.57 Per-Cent
at 0.000
Energy (MeV)

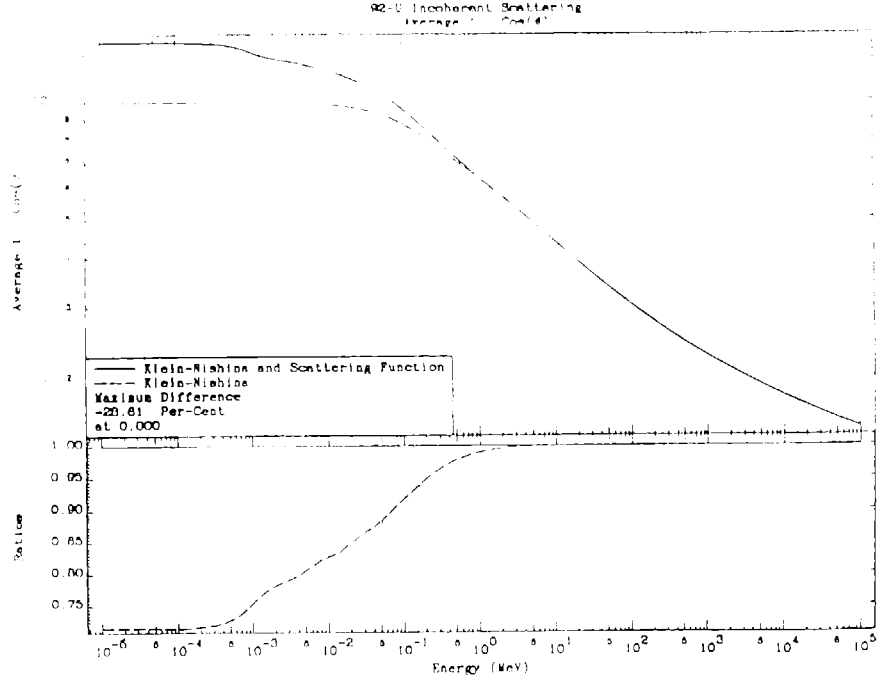
92-U Incoherent Scattering
Klein-Nishina and Scattering Function
Klein-Nishina
Maximum Difference
-20.61 Per-Cent
at 0.000
Ratio
Energy (MeV)

Fig. 2C

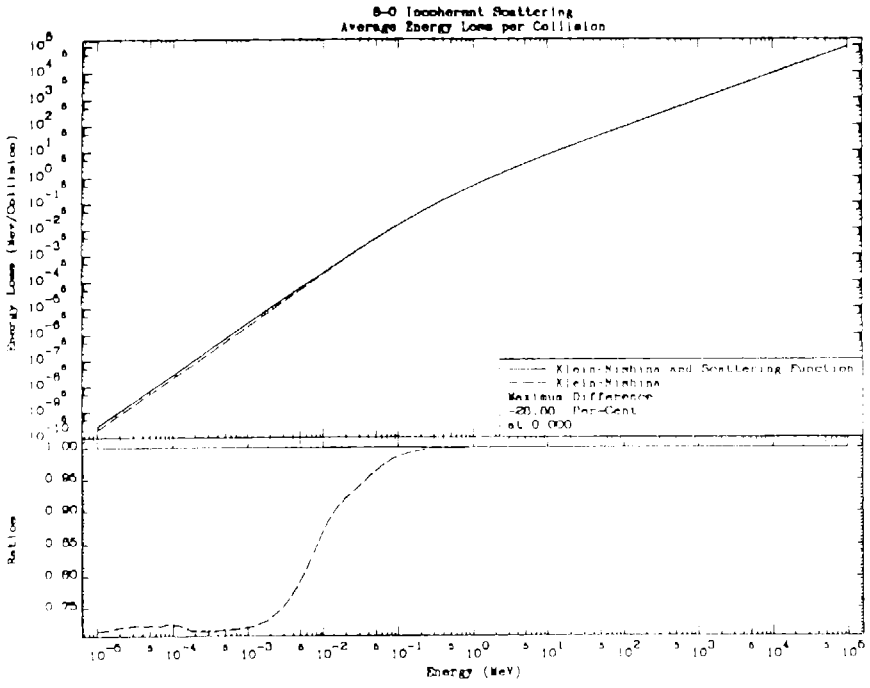
8-O Incoherent Scattering
Average Energy Loss per Collision
Energy Loss (Mev/Collision)
Klein-Nishina and Scattering Function
Klein-Nishina
Maximum Difference
-28.00 Per-Cent
at 0.000
Ratios
Energy (MeV)

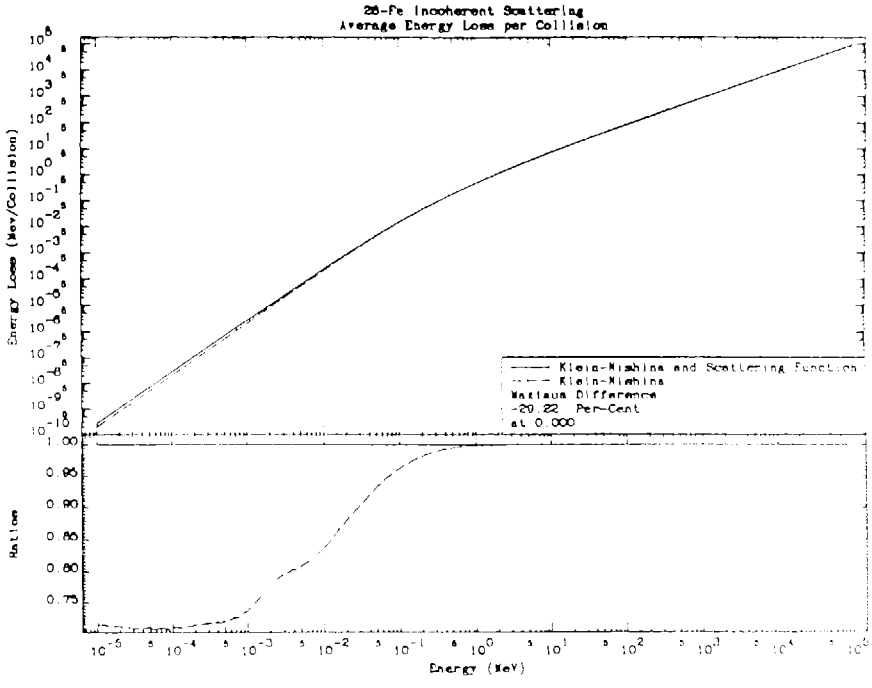
26-Fe Incoherent Scattering
Average Energy Loss per Collision
Energy Loss (Mev/Collision)
Klein-Nishina and Scattering Function
Klein-Nishina
Maximum Difference
-29.22 Per-Cent
at 0.000
Ratios
Energy (MeV)

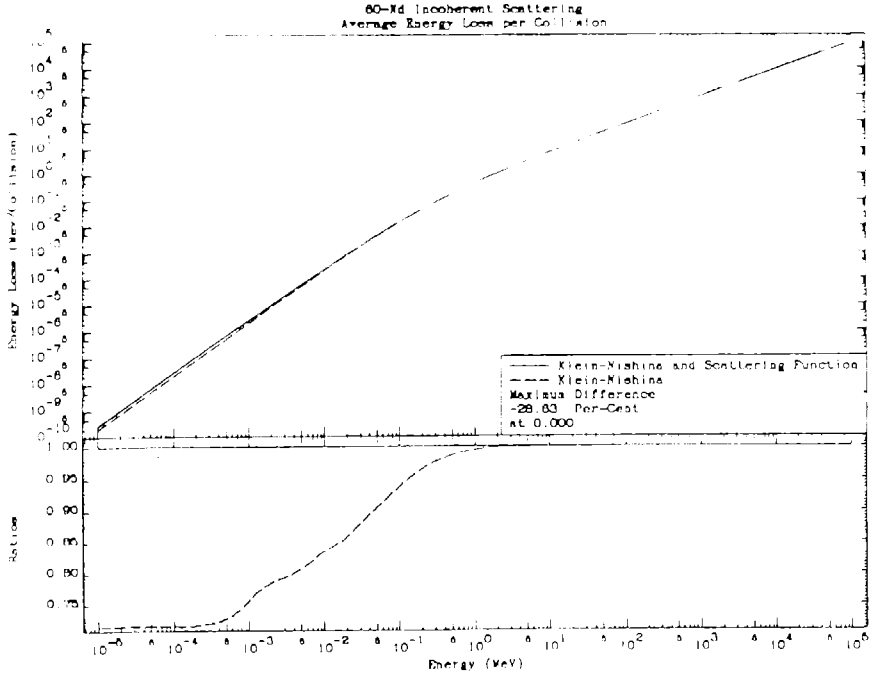
60-Nd Incoherent Scattering
Average Energy Loss per Collision
Energy Loss (Mev/Collision)
Klein-Nishina and Scattering Function
Klein-Nishina
Maximum Difference
-28.03 Per-Cent
at 0.000
Ratios
Energy (MeV)

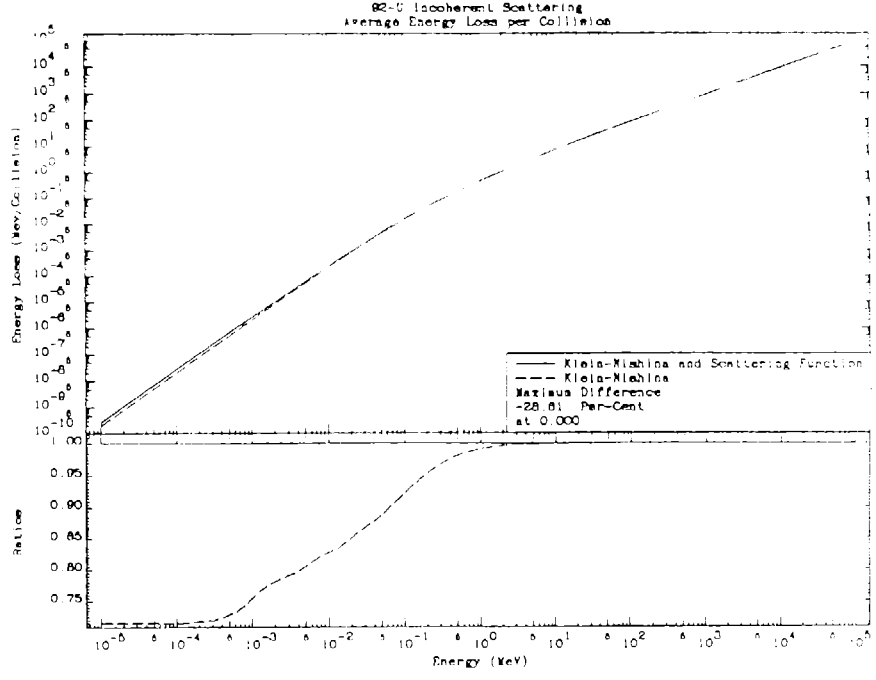
92-U Incoherent Scattering
Average Energy Loss per Collision
Energy Loss (Mev/Collision)
Klein-Nishina and Scattering Function
Klein-Nishina
Maximum Difference
-28.61 Per-Cent
at 0.000
Ratios
Energy (MeV)

Fig. 21

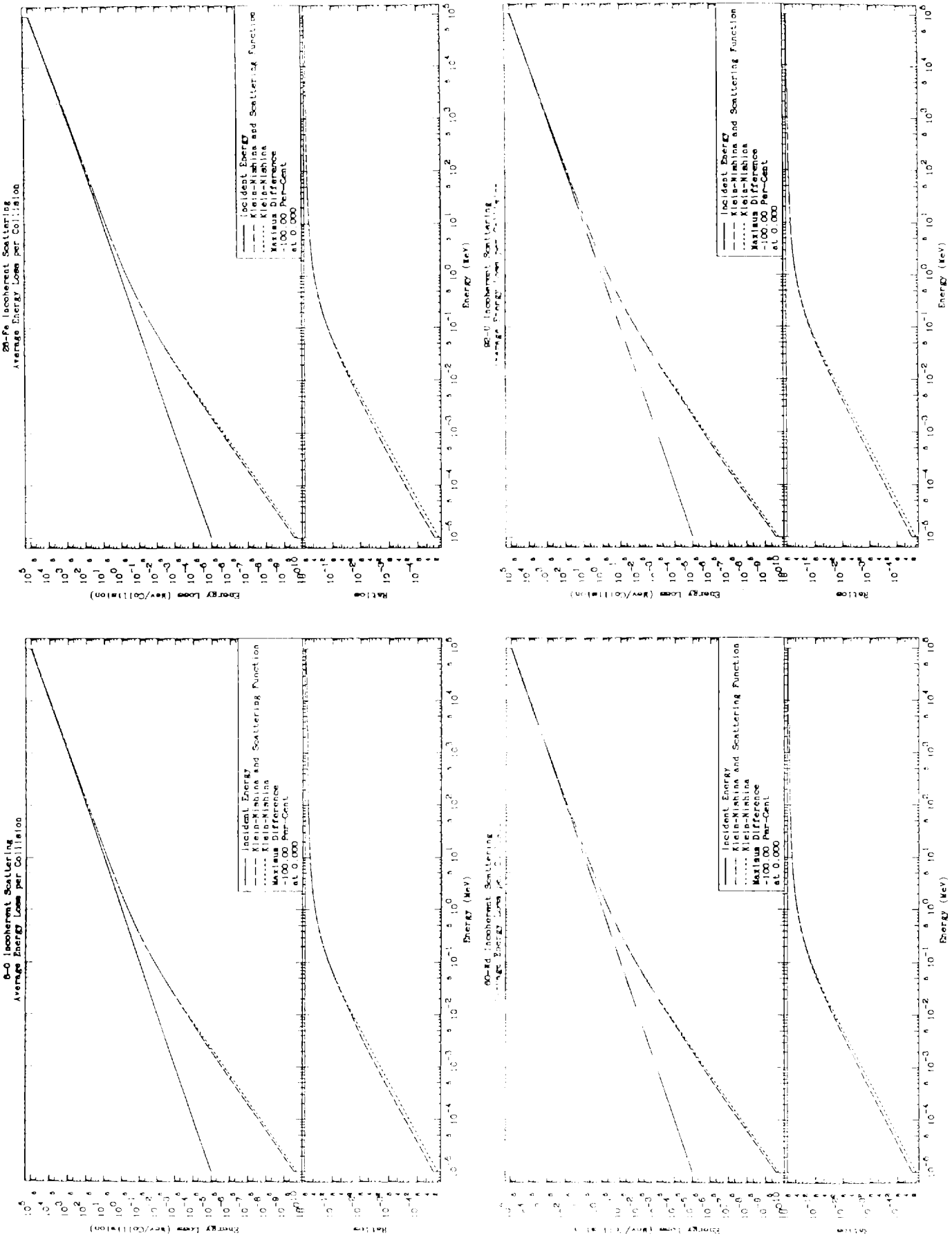
Incident Energy
Klein-Nishina and Scattering Function
Klein-Nishina
Maximum Difference
-100.00 Per-Cent
at 0.000
Energy (KeV)
Ratio

FIG. 22

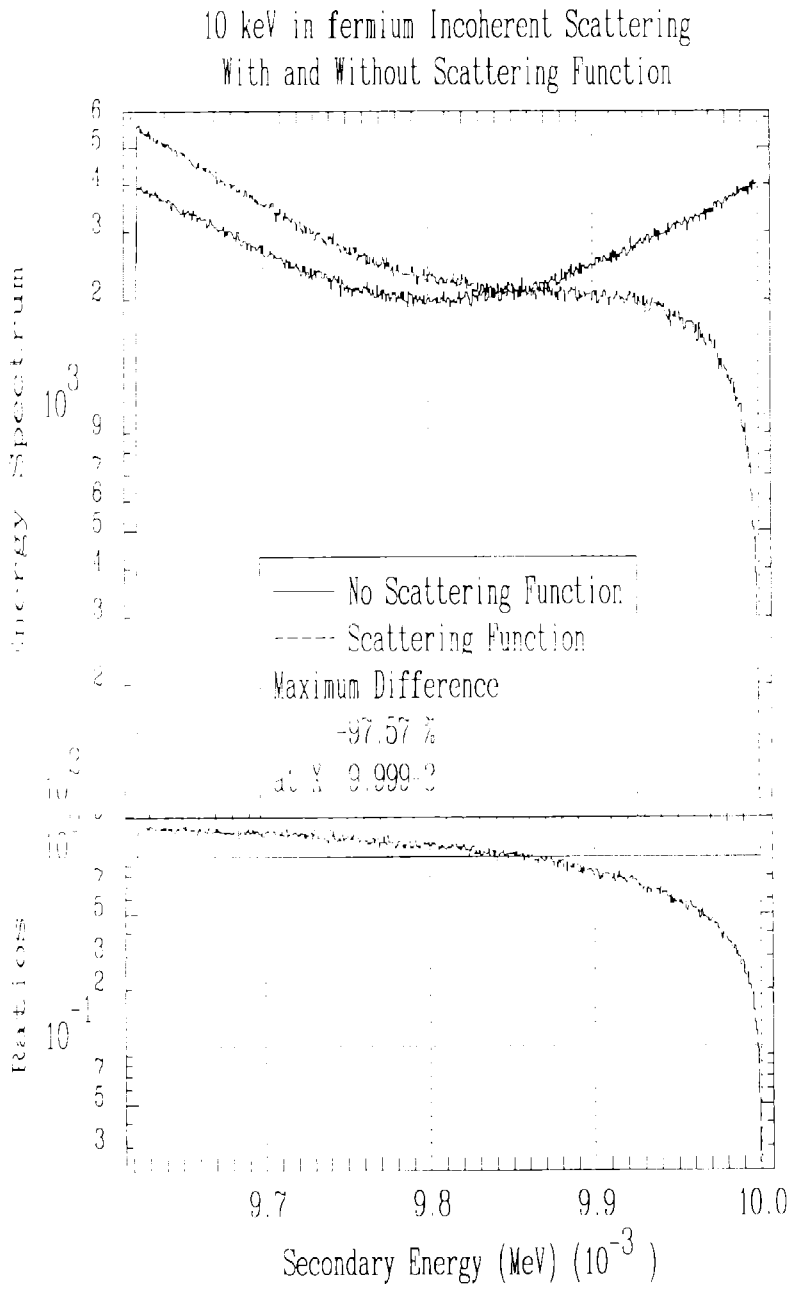
10 keV in fermium Incoherent Scattering
With and Without Scattering Function
No Scattering Function
Scattering Function
Maximum Difference
-97.57 %
9.999-3
Ratios
9.7
9.8
9.9
10.0
Secondary Energy (MeV) (10^{-3})

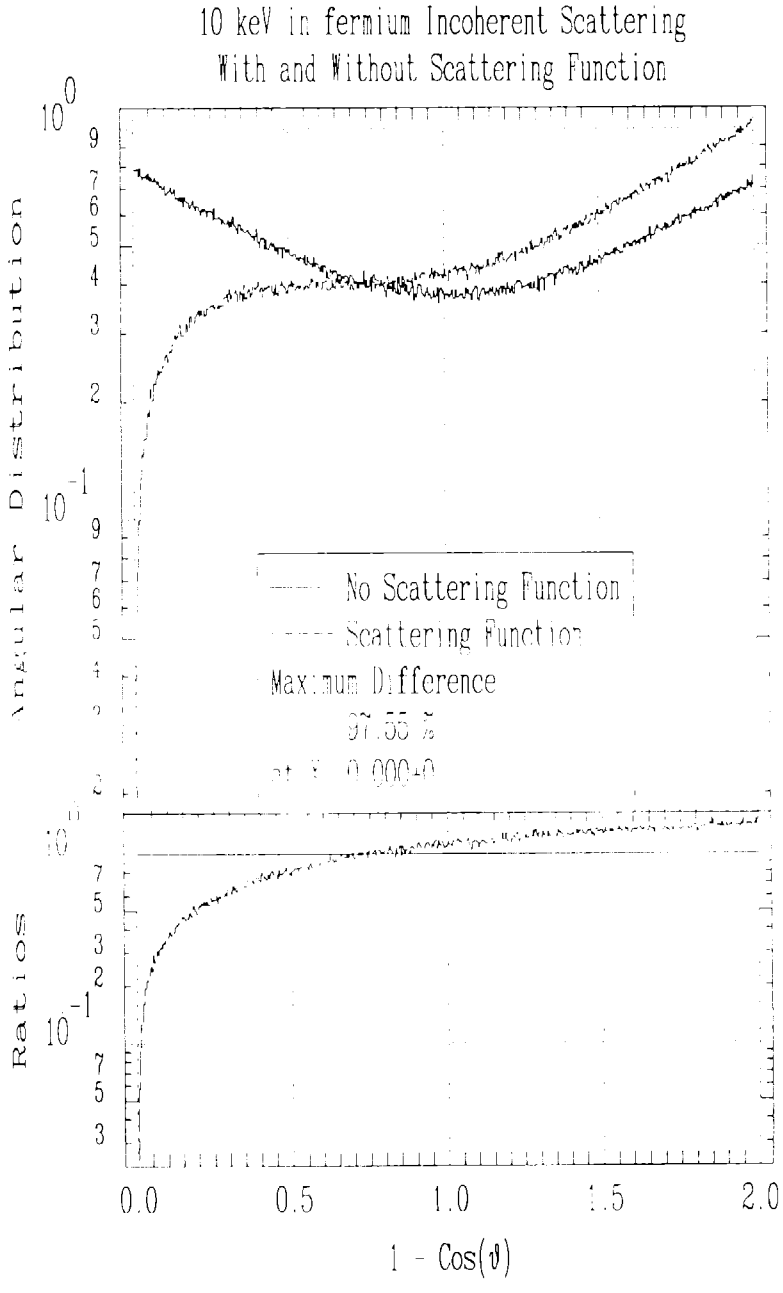
10 keV in fermium Incoherent Scattering
With and Without Scattering Function
Angular Distribution
No Scattering Function
Scattering Function
Maximum Difference
Ratios
0.0
0.5
1.0
1.5
2.0
1 - Cos(ϑ)

FIG. 23

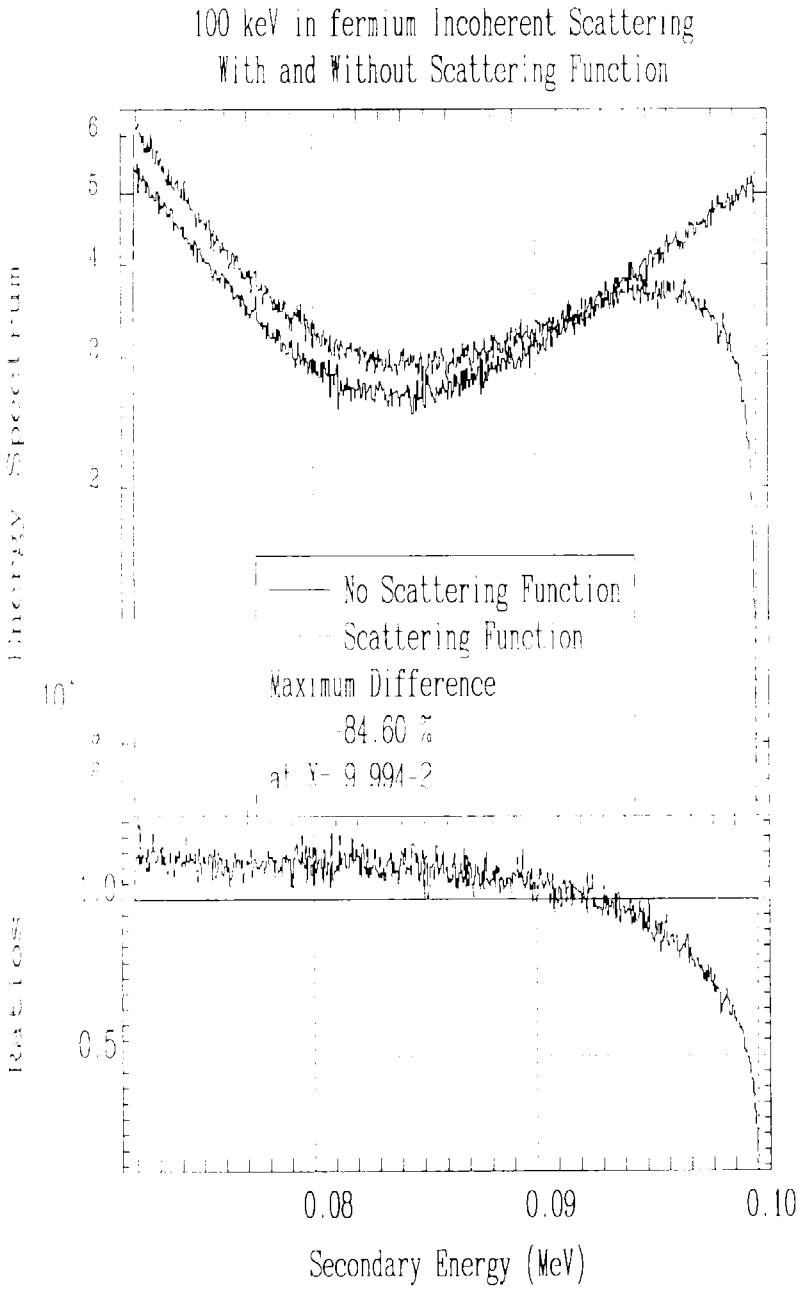
100 keV in fermium Incoherent Scattering
With and Without Scattering Function
No Scattering Function
Scattering Function
Maximum Difference
84.60 %
Ratios
0.08
0.09
0.10
Secondary Energy (MeV)

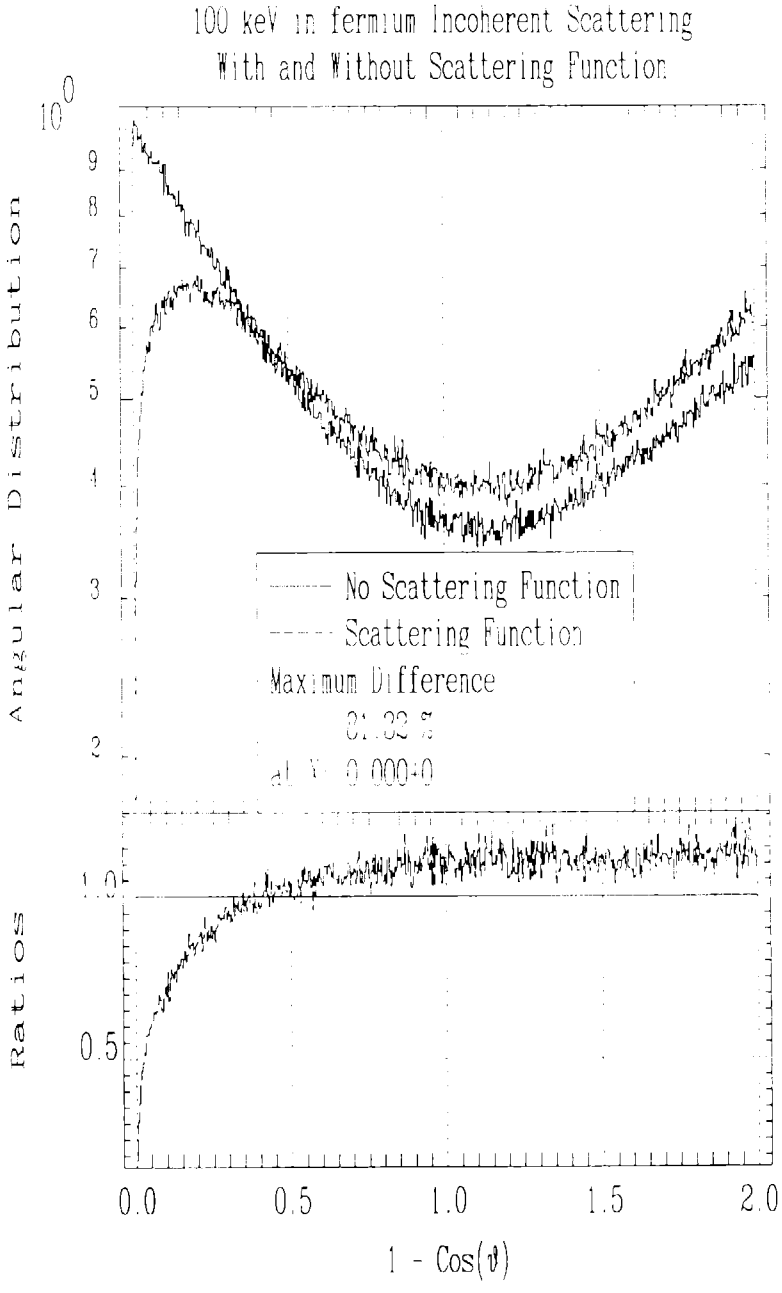
100 keV in fermium Incoherent Scattering
With and Without Scattering Function
Angular Distribution
No Scattering Function
Scattering Function
Maximum Difference
Ratios
0.0
0.5
1.0
1.5
2.0
1 - Cos(ϑ)

Fig. 24

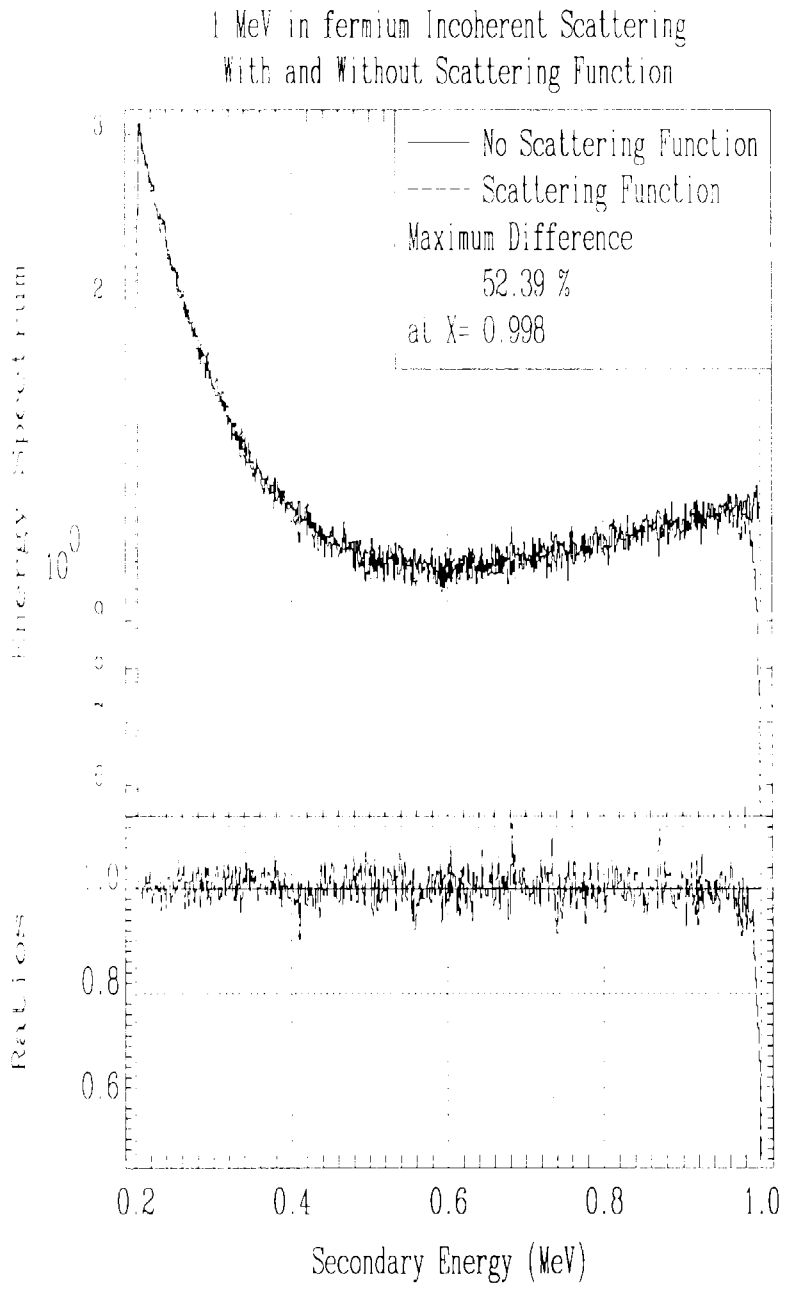
1 MeV in fermium Incoherent Scattering
With and Without Scattering Function
No Scattering Function
Scattering Function
Maximum Difference
52.39 %
at X= 0.998
Ratios
0.8
0.6
0.2
0.4
0.6
0.8
1.0
Secondary Energy (MeV)

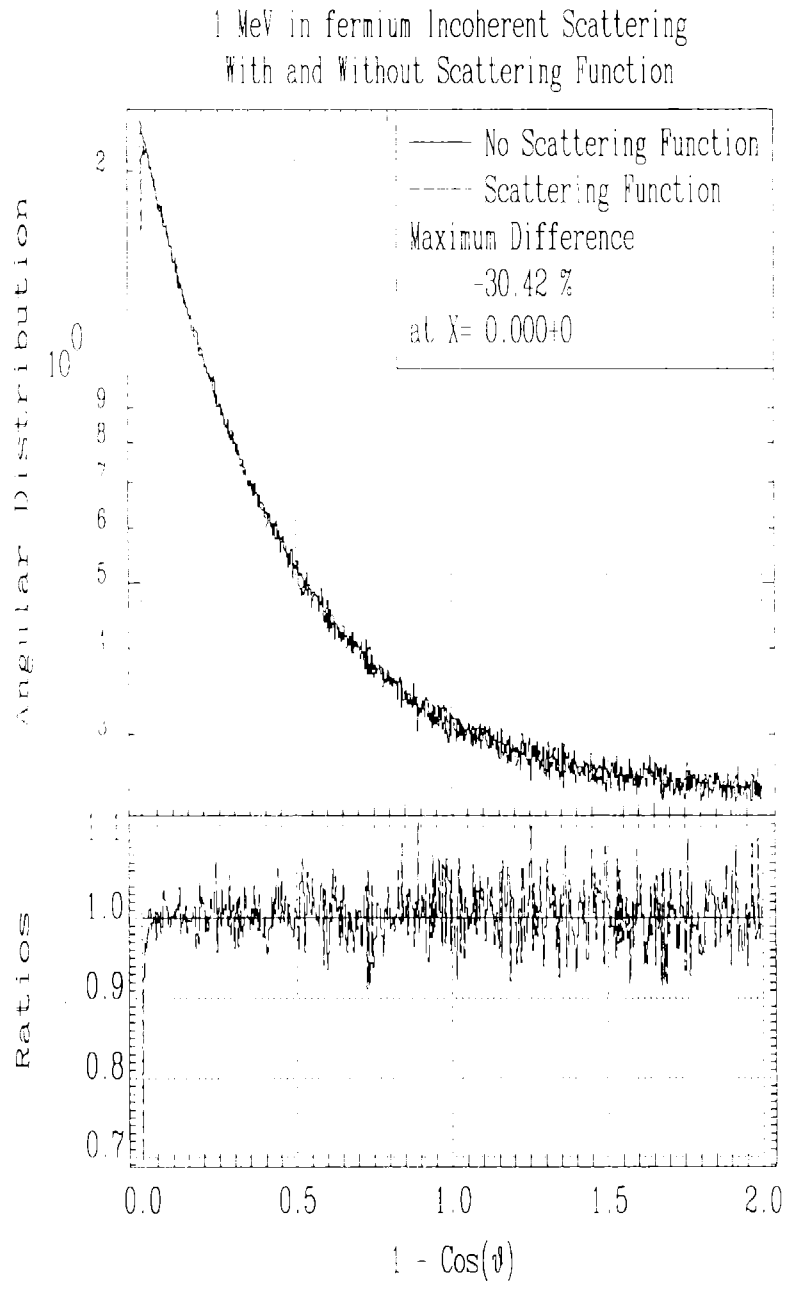
1 MeV in fermium Incoherent Scattering
With and Without Scattering Function
No Scattering Function
Scattering Function
Maximum Difference
-30.42 %
at X= 0.000+0
Angular Distribution
Ratios
0.9
0.8
0.7
0.0
0.5
1.0
1.5
2.0
1 - Cos(ϑ)

FIG. 25